Calculation of photonic bands using vector cylindrical waves and reflectivity of light for an array of dielectric rods

Kazuo Ohtaka,* Tsuyoshi Ueta, and Katsuki Amemiya
Department of Applied Physics, Faculty of Engineering, Chiba University, 1-33 Yayoi-cho, Inage-ku, Chiba 263, Japan
(Received 19 August 1997)

For a periodic array of dielectric rods of circular cross section, the formulation is given for the band structure of a photon and the reflectivity or transmittivity of light, using the vector cylindrical waves as the basis function for expansion. As a key quantity assuring the fast convergence, the expression of the structure factor is given for two- and three-dimensional arrays and for a lattice with a complex unit cell containing a number of rods inside. In terms of the calculated band energies, we check the reliability of the widely used plane-wave methods and estimate the error involved in them. Also, we present some numerical results for the band structure and the transmittivity of light for parameters beyond the reach of the plane-wave approach. [S0163-1829(98)05804-4]

I. INTRODUCTION

Because of the accumulated knowledge of the basic properties of the photonic band,[1,2] a stage of their application seems to be beginning both theoretically and technologically.[3–7] Though most theoretical work is done using the complete set of plane waves as basis functions, the experience for electrons reveals that the set of spherical waves is much more powerful in leading to a faster convergence. It is true that their usefulness is restricted to arrays of spherical substances but the conclusions drawn sometimes even analytically give us sufficient insight into the physics of more complicated photonic crystals, an array of rectangular rods, for example. Indeed, as shown in the series of works for the arrayed spheres of dielectrics,[8–11] the calculated eigenvalues and eigenvectors of very high quality clarified the origin of the characteristic features of individual bands. The strong confinement effect that gives rise to an enhanced local field is one of the examples that convinces us of the existence of the similar effect irrespective of the shape and size of the arrayed dielectrics.

The need of the fast convergence is connected with the presence of the virtual bound states of photons confined to a dielectric unit, i.e., the origin of the Mie resonance in the light-matter interaction. In a periodic array of dielectrics, the bound states of different units are coupled, as in a tight-binding band of electrons, to become a well-defined coherent wave with massive dispersion relations. This mode is nothing but a bosonic analogue of heavy fermions,[8,12] and is called in this paper and elsewhere heavy photon, as in the works cited above for the lattice of spheres. Their peculiar feature is that the confinement effect becomes more and more conspicuous with higher angular momentum l ($\hbar=1$)—in the language of electrons. In the morphology-dependent lasing in the cavity quantum electrodynamics (QED),[13] the gallery modes with l as large as 30 are indeed involved. If the perfect periodicity is somehow assured, they will manifest themselves as high-energy heavy photons, now coherent and free from a radiative lifetime effect. This is in a marked contrast to the case of electrons, where it is only in the energy range of the d or f state (i.e., $l=2$ or 3), that heavy fermions have so far been observed. We wish to have a powerful algorithm to cover the heavy photons of such a high-energy region.

A good localization of impurity modes seems to be another reason for the need of fast convergence.[14,15] In contrast to the donor or acceptor levels of electrons, the high degree of localization of the photonic analogues almost nullifies the effective mass equation. The supercell method[16,17] looks to be a promising alternative. A unit cell thereof that contains a large number of dielectrics introduces a secular matrix with dimensions orders of magnitude larger than the perfect system.

The purpose of this paper is to give such a formulation for a lattice formed by parallel dielectric rods of a circular cross section. For two- and three-dimensional (3D) arrays of dielectric spheres, the readers should refer to the works of one of the present authors.[8–11] The attempts along this line for the array of rods are already found in the series of works of Nicorovici and co-workers.[18–20] They are thus credited with having first developed the cylindrical wave formalism. They concentrated on the multipolar expansion of the Green function and gave the algorithm for the structure factor, in the terminology of the present paper, for 1D, 2D, and 3D periodic lattices. They applied it to the calculation of the photonic band for the arrays of perfectly conducting cylinders and spheres. In these systems, the scalar wave treatment was possible and no essential change except the boundary condition was needed in the scalar Korringa-Kohn-Rostoker (KKR) equation. We give in this paper the full vector KKR equation. This equation is an extension to the cylindrical case of the vector KKR equation given for the array of spheres.[21] Also, the formalism for the transmission and the reflection coefficients, the response of photonic bands to an incident optical probe, is also given.

In the formulation of the structure factor, there are a number of differences between the works of Nicorovici and coworkers and the present paper. The structure factor for a monolayer of parallel cylinders was given by them in a kind of recursion form for a set of S_l, defined in the text.[18] In this

paper we are giving a closed expression of S_l for each l. The structure factor of the monolayer is the most important ingredient to obtain the reflectivity or transmittivity of light from a system of stacking planes of rods. We are giving also the expression of S_l for an infinite 3D system having a number of rods in a unit cell, with the future application to the supercell method in mind. One important point is that the algorithm for S_l of the 3D system of Nicorovici and coworkers does not rely upon the Ewald method in the lattice sums, in contrast to the conventional way.[19,20] Thus a very interesting and important problem remains to be examined; that is, whether their expression works better than the conventional one, in a very-high-frequency region as stated above.

As in the case of arrayed spheres,[8,21] the formulation for the photonic bands ends in a set of formulas that are obtained through a simple transformation applied to the results for electrons. What matters in the formulation is to establish the completeness relation of the vector cylindrical waves and to use it just as the closure relation for electrons written in terms of bras and kets. In this sense the difference in the formalism is very small between electrons and photons. To show these points is the main reason for the detailed presentation of the formulation.

Our formulation will be applied numerically in two ways in this paper. First we examine the convergence of the band energies obtained by the plane-wave calculations by comparing them with the results of the present formulation. As Sözüer, Haus, and Inguva emphasized,[22] correct band energies of the plane-wave expansion must be obtained through the extrapolation procedure to the infinite number of the plane waves used in the expansion. If we wish to omit this formidable task, we have recourse to some other ways of estimating the errors due to the finite truncation. This is just what we are doing in this paper for several cases of different dielectric constants and frequency ranges. Our conclusion is that to attain a high precision the dimension of the secular matrix of the plane-wave calculation needs to be 50, sometimes more than 100, times as large as that of the cylindrical-wave formulation.

The second application concerns an ideal photonic crystal with finite thickness. We show how well the transmission and reflection of light is capable of reproducing the detailed features of the band structure. This second application is made for the parameters beyond the reach of the plane-wave calculations, using the numerical data calculated with errors less than 0.1% for about 80 bands of the system with large dielectric constants.

In Sec. II, we examine the basic properties of the vector cylindrical waves to establish the completeness relation. In Sec. III, we give the formulation for the calculations of band structure and reflectivity of light. Numerical applications are given in Secs. IV and V. We end the paper with a brief summary in Sec. VI. The detailed expression for the structure factors will be given in Appendixes A, B, and C. We treat a 2D plane, an infinite 3D lattice, and a lattice of complex unit cells having a number of cylinders.

II. COMPLETENESS OF THE VECTOR SPHERICAL WAVES

Generating the vector spherical waves from the scalar ones is well established and described in detail in various sources, among them Stratton.[23] For the solutions of the vector Helmholtz equation for the electric field,

$$(\Delta+q^2)\mathbf{E}(\mathbf{r})=0, \tag{2.1}$$

the relevant scalar function in the cylindrical coordinates $\mathbf{r}=(\rho,\theta,z)$ is

$$\psi_{lk_z}(\mathbf{r};C)=C_l(\lambda\rho)e^{il\theta}e^{ik_z z}, \tag{2.2}$$

with

$$\lambda=(q^2-k_z^2)^{1/2}. \tag{2.3}$$

The index l stands for the z component of the angular momentum and the symbol C may be J for the Bessel function J_l, H for the Hankel function $H_l^{(1)}$ of the first kind, or N for the Neumann function N_l. We let l run over $-\infty<l<\infty$ with the relation $C_{-l}(\lambda\rho)=(-1)^l C_l(\lambda\rho)$. Throughout the paper we take $\mathrm{Im}\lambda>0$ (when $q^2>k_z^2$, q is understood to be $q+i\delta$ with $q>0$ and $\delta=0+$).

For an l, three vector cylindrical waves are constructed from $\psi_{lk_z}(\mathbf{r})$. Two of them, the M and N fields of Stratton, are *transverse* fields in the sense that $\nabla\cdot\mathbf{E}(\mathbf{r})=0$. Let them be $\boldsymbol{\epsilon}_l^M(\mathbf{r})$ and $\boldsymbol{\epsilon}_l^N(\mathbf{r})$, respectively. The third, the L-type field, is *longitudinal* and denoted as $\boldsymbol{\epsilon}^L(\mathbf{r})$. The M wave is alternatively called the transverse electric field and the N the transverse magnetic field (they are also called the magnetic and electric multipole fields, respectively).[24] The L field disappears finally in our problem but it is indispensable in setting up the closure relation, as shown below.

The concrete forms of the (ρ,θ,z) components of $\boldsymbol{\epsilon}_l^M(\mathbf{r};C)$, etc., are

$$\boldsymbol{\epsilon}_l^M(\mathbf{r};C)=\frac{1}{\lambda}\left(\frac{1}{\rho}\frac{\partial}{\partial\theta},-\frac{\partial}{\partial\rho},0\right)\psi_{lk_z}(\mathbf{r};C),$$

$$\boldsymbol{\epsilon}_l^N(\mathbf{r};C)=\frac{1}{\lambda}\left(\frac{ik_z}{q}\frac{\partial}{\partial\rho},\frac{ik_z}{q}\frac{1}{\rho}\frac{\partial}{\partial\theta},\frac{\lambda^2}{q}\right)\psi_{lk_z}(\mathbf{r};C),$$

$$\boldsymbol{\epsilon}_l^L(\mathbf{r};C)=\frac{1}{\lambda}\left(\frac{\partial}{\partial\rho},\frac{1}{\rho}\frac{\partial}{\partial\theta},ik_z\right)\psi_{lk_z}(\mathbf{r};C). \tag{2.4}$$

They are dimensionless by definition. The lack of the z component discriminates the M field from the N and the generator of the L field is nothing but the gradient operator divided by λ.

The normalization integrals with respect to the angle θ turn out to be

$$\int_0^{2\pi}d\theta\boldsymbol{\epsilon}_l^L(\mathbf{r};C)^*\cdot\boldsymbol{\epsilon}_{l'}^L(\mathbf{r};C)=\pi\delta_{ll'}[C_{l-1}^2+C_{l+1}^2+2(k_z/\lambda)^2C_l^2],$$

$$\int_0^{2\pi}d\theta\boldsymbol{\epsilon}_l^M(\mathbf{r};C)^*\cdot\boldsymbol{\epsilon}_{l'}^M(\mathbf{r};C)=\pi\delta_{ll'}[C_{l-1}^2+C_{l+1}^2],$$

$$\int_0^{2\pi}d\theta\boldsymbol{\epsilon}_l^N(\mathbf{r};C)^*\cdot\boldsymbol{\epsilon}_{l'}^N(\mathbf{r};C)=\pi\delta_{ll'}[(k_z/q)^2(C_{l-1}^2+C_{l+1}^2)+2(\lambda/q)^2C_l^2]. \tag{2.5}$$

With respect to the angle integral they are not mutually orthogonal but

$$\int_0^{2\pi} d\theta \boldsymbol{\epsilon}_l^L(\mathbf{r};C)^* \cdot \boldsymbol{\epsilon}_{l'}^M(\mathbf{r};C) = i\pi\delta_{ll'}[C_{l-1}^2 - C_{l+1}^2],$$

$$\int_0^{2\pi} d\theta \boldsymbol{\epsilon}_l^L(\mathbf{r};C)^* \cdot \boldsymbol{\epsilon}_{l'}^N(\mathbf{r};C) = i\pi\delta_{ll'}(k_z/q) \times [C_{l-1}^2 + C_{l+1}^2 - 2C_l^2],$$

$$\int_0^{2\pi} d\theta \boldsymbol{\epsilon}_l^M(\mathbf{r};C)^* \cdot \boldsymbol{\epsilon}_{l'}^N(\mathbf{r};C) = \pi\delta_{ll'}(k_z/q)[C_{l-1}^2 - C_{l+1}^2]. \tag{2.6}$$

The third relation causes the mixing between the M and N partial waves in the case of $k_z \neq 0$, to be discussed in Sec. III B. This is in a marked contrast to the scattering from a sphere,[8] where the M and N fields decouple to lead to the M and N phase shifts.

There are three important identities needed in the calculus of the vector cylindrical waves. One is related to the Cartesian components of their superpositions. The Cartesian components of $\boldsymbol{\epsilon}_l^M(\mathbf{r};J)$, etc. follow from Eq. (2.4). Let $\mathbf{E}(\mathbf{r})$ be a superposition of M and N waves over l with coefficients α_l^M and α_l^N;

$$\mathbf{E}(\mathbf{r};C) = \sum_{l=-\infty}^{\infty} \{\boldsymbol{\epsilon}_l^M(\mathbf{r};C)\alpha_l^M + \boldsymbol{\epsilon}_l^N(\mathbf{r};C)\alpha_l^N\}. \tag{2.7}$$

This is a transverse field, because so are $\boldsymbol{\epsilon}_l^M$ and $\boldsymbol{\epsilon}_l^N$. When expanded in terms of the scalar function given by Eq. (2.2), its ith Cartesian component ($i = x,y,z$) is expressed as

$$E_i(\mathbf{r};C) = \sum_{ll'} \{\psi_{lk_z}(\mathbf{r};C)[\mathbf{P}_i^M]_{ll'}\alpha_{l'}^M + \psi_{lk_z}(\mathbf{r};C)[\mathbf{P}_i^N]_{ll'}\alpha_{l'}^N\}. \tag{2.8}$$

This shows that to derive the ith component we have only to change α_l^β in $\mathbf{E}(\mathbf{r})$ by $\Sigma_{l'}[\mathbf{P}_i^\beta]_{ll'}\alpha_{l'}^\beta$ for $\beta = M,N$ and to superpose the scalar fields. When, in particular, $\mathbf{E}(\mathbf{r};C) = \boldsymbol{\epsilon}_l^M(\mathbf{r};C)$, only the matrix $\mathbf{P}_i^M$ enters with $\alpha_{l'}^\beta = \delta_{l'l}\delta_{\beta M}$ in the above formula. The equivalence of Eq. (2.7) with Eq. (2.8) is important in what follows. The matrices $\mathbf{P}_i^\beta$, whose ll' matrix elements are denoted as $[\mathbf{P}_i^\beta]_{ll'}$, are playing a fundamental role in converting the scalar (Schrödinger) equation to the vector (Maxwell) version. Their explicit forms are quite simple in the cylindrical case, as compared with the spherical case where the Clebsch-Gordan coefficients are involved:[21]

$$\mathbf{P}_x^M = = \frac{i}{2}[1,1], \quad \mathbf{P}_y^M = \frac{1}{2}[1,-1], \quad \mathbf{P}_z^M = [0],$$

$$\mathbf{P}_x^N = \frac{ik_z}{2q}[-1,1], \quad \mathbf{P}_y^N = \frac{k_z}{2q}[-1,-1], \quad \mathbf{P}_z^N = \frac{\lambda}{q}[1]. \tag{2.9}$$

Here a of the notation $[a,b]$ stands for the $(l,l-1)$ matrix element and b the $(l,l+1)$ element, while the symbol $[a]$ shows the diagonal element (l,l) $(-\infty < l < \infty)$. The other matrix elements are zero identically.

The second important relation is

$$\frac{\partial}{\partial x_i}\sum_l \psi_{lk_z}(\mathbf{r};C)\xi_l = \sum_{ll'} \psi_{lk_z}(\mathbf{r};C)\lambda[\mathbf{Q}_i]_{ll'}\xi_{l'}, \tag{2.10}$$

ξ_l being an arbitrary coefficient independent of x_i. That is, when operated on a superposition of the cylindrical waves, the derivative with respect to x_i is equivalent to multiplying λ times the third matrix $\mathbf{Q}_i$. They are defined by

$$\mathbf{Q}_x = \tfrac{1}{2}[-1,1], \quad \mathbf{Q}_y = \frac{i}{2}[1,1], \quad \mathbf{Q}_z = \frac{ik_z}{\lambda}[1], \tag{2.11}$$

in the notation of Eq. (2.9).

The final and most important relation is the completeness (closure) relation established among $\mathbf{P}_i^M$, $\mathbf{P}_i^N$, and $\mathbf{Q}_i$ (nine matrices altogether). The completeness is proved in the same way as the spherical case.[21] Explicit matrix multiplication using Eqs. (2.9) and (2.11) actually leads to

$$\left[\sum_{\beta=M,N} \mathbf{P}_i^\beta(\mathbf{P}_j^\beta)^\dagger + \frac{\lambda^2}{q^2}\mathbf{Q}_i(\mathbf{Q}_j)^\dagger\right]_{ll'} = \delta_{ll'}\delta_{ij}, \tag{2.12}$$

the left-hand side being the (ll') matrix element.

This is called the completeness relation because it resolves an arbitrary vector field into a linear superposition of the M, N, and L vector cylindrical waves. This is illustrated by the following two examples.

The first example is resolving the plane wave of wave vector $\mathbf{k}$, transverse or longitudinal:

$$\mathbf{E}(\mathbf{r}) = \mathbf{E}^0 \exp(i\mathbf{k}\cdot\mathbf{r}), \tag{2.13}$$

with $\mathbf{E}^0 = (E_x^0, E_y^0, E_z^0)$. We rewrite the exponential in terms of the scalar cylindrical waves as follows:

$$e^{i(k_x x \pm k_y y)} = e^{ik_\perp \rho\cos(\theta(\mathbf{k}^\pm)-\theta)} = \sum_{l=-\infty}^{\infty} i^l J_l(k_\perp\rho)e^{-il(\theta(\mathbf{k}^\pm)-\theta)}. \tag{2.14}$$

Here

$$k_\perp = (k_x^2 + k_y^2)^{1/2} \tag{2.15}$$

and

$$e^{i\theta(\mathbf{k}^\pm)} = \frac{k_x \pm ik_y}{k_\perp}, \tag{2.16}$$

with $\theta(\mathbf{k}^\pm)$ being the angle between the 2D vector $\mathbf{k}^\pm = (k_x, \pm k_y)$ and the x axis (the last form of the exponential is useful for complex k_y). The field component of Eq. (2.13) is then rewritten as follows:

$$E_i(\mathbf{r}) = \sum_l i^l j_l(k_\perp\rho)e^{il\theta}e^{ik_z z}e^{-il\theta(\mathbf{k})}E_i^0 = \sum_{ll'}\sum_j \psi_{lk_z}(\mathbf{r};J(k_\perp\rho))\delta_{ll'}\delta_{ij}i^{l'}e^{-il'\theta(\mathbf{k})}E_j^0. \tag{2.17}$$

Substituting Eq. (2.12) for $\delta_{ll'}\delta_{ij}$ and using the equivalence between Eqs. (2.7) and (2.8), we find

$$\mathbf{E}^0 e^{i\mathbf{k}\cdot\mathbf{r}} = \sum_l \{\boldsymbol{\epsilon}_l^M(\mathbf{r};J(k_\perp\rho))\alpha_l^M + \boldsymbol{\epsilon}_l^N(\mathbf{r};J(k_\perp\rho))\alpha_l^N + \boldsymbol{\epsilon}_l^L(\mathbf{r};J(k_\perp\rho))\alpha_l^L\} \tag{2.18}$$

with the coefficients

$$\alpha_l^\beta = \sum_{l'} \left(\sum_j [(\mathbf{P}_j^\beta)^\dagger]_{ll'} E_j^0 \right) i^{l'} e^{-il'\theta(\mathbf{k})} \quad (\text{for } \beta = M,N)$$

$$\alpha_l^L = \sum_{l'} \left(\frac{\lambda^2}{k^2} \sum_j [(\mathbf{Q}_j^\beta)^\dagger]_{ll'} E_j^0 \right) i^{l'} e^{-il'\theta(\mathbf{k})}. \tag{2.19}$$

In deriving the L contribution, we note that the third matrix $\mathbf{Q}_i$ generates the ith component of the L wave, as $\mathbf{P}_i^M$ and $\mathbf{P}_i^N$ generated those of the M and N waves, respectively. This may be seen immediately from Eqs. (2.4) and (2.10) (in this sense, $\mathbf{Q}_i$ may as well be denoted as $\mathbf{P}_i^L$). The explicit forms of α_l^β and α_l^L given above are easily written down, since the matrices $\mathbf{P}_i^\beta$ and $\mathbf{Q}_i$ are simply given by Eqs. (2.9) and (2.11), respectively. For example, we find

$$\alpha_l^M = \mathrm{Im}(e^{i\theta(\mathbf{k})}\mathbf{E}_-^0) i^{l-1} e^{-il\theta(\mathbf{k})} \tag{2.20}$$

with

$$\mathbf{E}_-^0 = E_x^0 - iE_y^0. \tag{2.21}$$

Equation (2.18) shows that the plane-wave vector field, Eq. (2.13), is resolved into three cylindrical waves of various l. Any vector field, if it is expressed as a superposed vector plane-waves over $\mathbf{k}$, is thus reexpressed using the vector cylindrical waves. This is the expansion theorem we are concerned with here. If, in particular, the field $\mathbf{E}(\mathbf{r})$ is transverse, the L field does not mix, because the expansion coefficient α_l^L of Eq. (2.19) involves the matrix $\Sigma_j \mathbf{Q}_j E_j^0$ [note that $(\mathbf{Q}_j)^\dagger = -\mathbf{Q}_j$], which is, by Eq. (2.10), just the representation of $\boldsymbol{\nabla}\cdot\mathbf{E}(\mathbf{r})/\lambda$ and hence vanishes.

The second example of the use of the closure relation concerns the transformation of the quantity

$$\left(\delta_{ij} + \frac{1}{q^2}\frac{\partial^2}{\partial x_i \partial x_j} \right) \sum_l \psi_{lk_z}(\mathbf{r};C)\xi_l \tag{2.22}$$

with a constant amplitude ξ_l. The operator within the bracket is replaced by $\mathbf{Q}_i$ and $\mathbf{Q}_j$ via Eq. (2.10). The completeness relation Eq. (2.12) then leads to

$$\text{Eq. (2.22)} = \sum_l \psi_{lk_z}(\mathbf{r};C) \times \left(\sum_{\beta=M,N} \sum_{l'l''} [\mathbf{P}_i^\beta]_{ll'} [(\mathbf{P}_j^\beta)^\dagger]_{l'l''} \right) \xi_{l''}. \tag{2.23}$$

Introducing the coefficient $\eta_{l'}^\beta$ by

$$\eta_l^\beta = \sum_{l'} [(\mathbf{P}_j^\beta)^\dagger]_{ll'} \xi_{l'}, \tag{2.24}$$

we find

$$\text{Eq. (2.22)} = \sum_l \{\boldsymbol{\epsilon}_l^M(\mathbf{r};C)\eta_l^M + \boldsymbol{\epsilon}_l^N(\mathbf{r};C)\eta_l^N\}. \tag{2.25}$$

To summarize, the operator $[\delta_{ij} + (1/q^2)(\partial/\partial x_i)(\partial/\partial x_j)]$ introduces the superposition of the transverse cylindrical waves. It is true that the three waves, $\boldsymbol{\epsilon}^L, \boldsymbol{\epsilon}^M$, and $\boldsymbol{\epsilon}^N$, are apparently unwieldy because of the nonorthogonality but they do not cause any serious trouble in what follows. This is due mostly to the completeness relation given by Eq. (2.12).

III. SCATTERING THEORY AND SECULAR EQUATION FOR THE BAND STRUCTURE

Suppose a plane-wave light $\mathbf{E}^0(\mathbf{r})$ of frequency ω is incident upon a parallel array of cylindrical rods. We take the z axis in the direction of cylinder axis and specify the center of the nth rod by the 2D coordinates $\mathbf{x}_n = (x_n, y_n)$. The 2D unit cell of the lattice of rods is assumed to have only one cylinder. The dielectric constant and radius of the cylinder are taken to be $\varepsilon_<$ and a, respectively. The array is assumed to be in free space. If it is embedded in a substance of dielectric constant $\varepsilon_>$, $\varepsilon_<$ and ω^2 in what follows are replaced by $\varepsilon_</\varepsilon_>$ and $\omega^2\varepsilon_>$, respectively.

Since the system considered in the light transmission is finite in the thickness direction and we are adopting the layer-doubling method to deal with the problem, we first examine the light scattering from a monolayer of dielectric cylinders lying in the xz plane.

A. Scattering from a monolayer of arrayed dielectrics

The layer-doubling method is a method of treating a finite system by repeating the monolayer scattering. Consider a monolayer of parallel rods with the x coordinate of the nth rod at $x_n = nd$, d being the spacing. One can show that the scattering problem of the Maxwell field is reduced to the following integral equation:[25]

$$E_i(\mathbf{r}) = E_i^0(\mathbf{r}) + \sum_j \int d\mathbf{r}' G_{ij}(\mathbf{r},\mathbf{r}') V(\mathbf{r}') E_j^<(\mathbf{r}'), \tag{3.1}$$

with the ''potential'' given by

$$V(\mathbf{r}) = -q^2[\varepsilon(\mathbf{r}) - 1] \tag{3.2}$$

with $(c=1)$

$$q = \omega. \tag{3.3}$$

Here $\varepsilon(\mathbf{r})$ is the dielectric constant at the position $\mathbf{r}$, so that

$$\varepsilon(\mathbf{r}) = \begin{cases} \varepsilon_< & \mathbf{r} \text{ inside the cylinders,} \\ 1 & \mathbf{r} \text{ outside.} \end{cases} \tag{3.4}$$

Thus, $V(\mathbf{r})$ works only inside the dielectrics in Eq. (3.1). The subscript $<$ is intended to emphasize that field in the integrand is an inside field. The Greenian G_{ij} in Eq. (3.1) is defined by

$$G_{ij}(\mathbf{r},\mathbf{r}')=\left(\delta_{ij}+\frac{1}{q^2}\frac{\partial^2}{\partial x_i\partial x_j}\right)G(\mathbf{r},\mathbf{r}'), \tag{3.5}$$

through the Green function G of the scalar Helmholtz equation. The operator in front of G is already familiar from Eq. (2.22). To take account of the periodic array of scatterers in the x direction, it is convenient to introduce, in place of G, the Green function G_{k_x} for the Bloch wave with wave number k_x in the x direction:[18]

$$\begin{aligned}G_{k_x}(\mathbf{r},\mathbf{r}')&=-\frac{1}{4\pi}\sum_n e^{ik_x x_n}\frac{\exp(iq|\mathbf{r}-\mathbf{r}'-\mathbf{x}_n|)}{|\mathbf{r}-\mathbf{r}'-\mathbf{x}_n|}\\&=\int\frac{dp_z}{2\pi}e^{ip_z(z-z')}[g^{(0)}(\boldsymbol{\rho},\boldsymbol{\rho}')+g^{(1)}(\boldsymbol{\rho},\boldsymbol{\rho}')].\end{aligned} \tag{3.6}$$

Here $\mathbf{r}=(\boldsymbol{\rho},z)=(\rho,\theta,z)$, $\mathbf{r}'=(\boldsymbol{\rho}',z')=(\rho',\theta',z')$, and k_x is equal to the x component of the incident wave vector, specified below. In the Fourier decomposition of the second line, the Green's function $g^{(0)}$ is the contribution from $n=0$ of the first line. It takes account of the singularity at $\mathbf{r}=\mathbf{r}'$ of the Green's function. The remaining $g^{(1)}$, the contribution from $n\neq 0$, incorporates the effects of the other rods into the structure factor Γ, which we call the scalar structure factor. It holds that

$$g^{(0)}(\boldsymbol{\rho},\boldsymbol{\rho}')=-\frac{i}{4}\sum_l H_l^{(1)}(\lambda\rho_>)J_l(\lambda\rho_<)e^{il\theta}e^{-il\theta'},$$

$$g^{(1)}(\boldsymbol{\rho},\boldsymbol{\rho}')=-\frac{i}{4}\sum_{l,l'} J_l(\lambda\rho)e^{il\theta}\Gamma_{ll'}(k_x,p_z)J_{l'}(\lambda\rho')e^{-il'\theta'}, \tag{3.7}$$

with

$$\lambda=[q^2-p_z^2]^{1/2}, \tag{3.8}$$

where $\rho_>$ ($\rho_<$) is the larger (smaller) of ρ and ρ'. By way of the structure factor $\Gamma_{ll'}$, $g^{(1)}$ depends on k_x. Note that in the integral over p_z, $\Gamma_{ll'}$ involves p_z through λ.

When this k_x-dependent Green's function is used in Eq. (3.5), the integral over $\mathbf{r}'$ of Eq. (3.1) can be restricted to a single cylinder, which is taken to be the one centered at $x_n=0$ [we call it the r (reference) cylinder].

For an incident light of wave number q and wave vector $\mathbf{k}$, we set

$$\mathbf{E}^0(\mathbf{r})=\mathbf{E}^0e^{i(k_xx+k_yy+k_zz)} \tag{3.9}$$

with $k^2=q^2$. The x component k_x is none other than the one used in defining G_{k_x} in the above. By symmetry the z dependence of any field is described everywhere by e^{ik_zz}. Thus by the integrals over z' in Eq. (3.1) and over p_z in Eq. (3.6), the component p_z is eventually replaced everywhere by k_z.

To solve Eq. (3.1), we note that the field inside the rods satisfies

$$(\Delta+q^2\varepsilon_<)E_j^<(\mathbf{r})=0, \tag{3.10}$$

that is,

$$V(\mathbf{r})E_j^<(\mathbf{r})=(\Delta+q^2)E_j^<(\mathbf{r}) \tag{3.11}$$

for $\mathbf{r}$ inside the r cylinder. Using this in Eq. (3.1), we can apply the Green's theorem in the integral of $\mathbf{r}'$. Integrating twice by parts leads then to the volume integral involving

$$(\Delta'+q^2)G(\mathbf{r},\mathbf{r}') \tag{3.12}$$

plus the integral over the surface of the r cylinder. Since the quantity of Eq. (3.12) is just $\delta(\mathbf{r}-\mathbf{r}')$, the volume integral is trivial. We thus obtain

$$0=\mathbf{E}^0(\mathbf{r})+\left(1+\frac{1}{q^2}\boldsymbol{\nabla}\boldsymbol{\nabla}\cdot\right)\mathbf{I}_{k_x}^<(\mathbf{r}) \tag{3.13}$$

for $\mathbf{r}$ inside and

$$\mathbf{E}_{k_x}^>(\mathbf{r})=\mathbf{E}^0(\mathbf{r})+\left(1+\frac{1}{q^2}\boldsymbol{\nabla}\boldsymbol{\nabla}\cdot\right)\mathbf{I}_{k_x}^<(\mathbf{r}) \tag{3.14}$$

for $\mathbf{r}$ outside the r cylinder. Here

$$\begin{aligned}\mathbf{I}_{k_x}^<(\mathbf{r})=\int_{\rho=a}d\mathbf{S}'\cdot\{&G_{k_x}(\mathbf{r},\mathbf{r}')\boldsymbol{\nabla}'\mathbf{E}^<(\mathbf{r}')\\&-[\boldsymbol{\nabla}'G_{k_x}(\mathbf{r},\mathbf{r}')]\mathbf{E}^<(\mathbf{r}')\}\end{aligned} \tag{3.15}$$

defines the surface integral. Once the inside field $\mathbf{E}_{k_x}^<(\mathbf{r})$ is determined from Eq. (3.13), the outside one is given via Eq. (3.14). The remaining task is thus to solve the former.

Let us set

$$\begin{aligned}\lambda_>&=(q_>^2-k_z^2)^{1/2},\\\lambda_<&=(q_<^2-k_z^2)^{1/2},\end{aligned} \tag{3.16}$$

with

$$\begin{aligned}q_>^2&=q^2,\\q_<^2&=q^2\varepsilon_<\end{aligned} \tag{3.17}$$

and denote the matrices $\mathbf{P}_j^\beta$ as $\mathbf{P}_j^{\beta>}$ and $\mathbf{P}_j^{\beta<}$, dependent upon which of the $(\lambda_>,q_>)$ and $(\lambda_<,q_<)$ is used in the definition of Eq. (2.9). In Eq. (3.13) let us resolve the incident field $\mathbf{E}_{k_x}^0(\mathbf{r})$ into the M and N partial waves following Eq. (2.18):

$$\mathbf{E}^0\exp(i\mathbf{k}\cdot\mathbf{r})=\sum_{\beta=M,N}\sum_l\boldsymbol{\epsilon}_l^\beta(\mathbf{r};J(\lambda_>\rho))\alpha_l^{\beta0} \tag{3.18}$$

with $\alpha_l^{\beta0}$ given by Eq. (2.19). The L wave does not appear because of the transversality. The Cartesian component of Eq. (3.18) is

$$E^0(\mathbf{r})_i=\sum_{\beta=M,N}\sum_{ll'}\psi_{lk_z}(\mathbf{r};J(\lambda_>\rho))[\mathbf{P}_i^{\beta>}]_{ll'}\alpha_{l'}^{\beta0}. \tag{3.19}$$

For the unknown inside field, we assume the form

$$\mathbf{E}^<(\mathbf{r})=\sum_{\beta=M,N}\sum_l\boldsymbol{\epsilon}_l^\beta(\mathbf{r};J(\lambda_<\rho))\alpha_l^{\beta<}, \tag{3.20}$$

with the ith component written as

$$E_i^<(\mathbf{r})=\sum_{\beta=M,N}\sum_{ll'}\psi_{lk_z}(\mathbf{r};J(\lambda_<\rho))[\mathbf{P}_i^{\beta<}]_{ll'}\alpha_{l'}^{\beta<}. \tag{3.21}$$

We put Eqs. (3.19) and (3.21) into Eq. (3.15). The angle integral of it is carried out using

$$\int_0^{2\pi} d\theta e^{i(l-l')\theta}=2\pi\delta_{ll'}. \tag{3.22}$$

The gradient operator introduces the factors

$$d_l^<=z_<H_l(z_>)J_l'(z_<)-z_>H_l'(z_>)J_l(z_<),$$

$$d_l^>=z_<J_l(z_>)J_l'(z_<)-z_>J_l'(z_>)J_l(z_<), \tag{3.23}$$

with $z_>=\lambda_>a$ and $z_<=\lambda_<a$. The former appears in the integral of $g^{(0)}$ and the latter in $g^{(1)}$. The operator in front of $\mathbf{I}_{k_x}^<(\mathbf{r})$ may be treated using the completeness relation, as done for the quantity of Eq. (2.22). In this way, from Eq. (3.13) we find

$$\sum_{\beta'=M,N}\sum_j\{(\mathbf{P}_j^{\beta>})^\dagger(\mathbf{D}^<+\boldsymbol{\Gamma}\mathbf{D}^>)\mathbf{P}_j^{\beta'<}\}\boldsymbol{\alpha}^{\beta'<}=-\frac{2i}{\pi}\boldsymbol{\alpha}^{\beta 0}, \tag{3.24}$$

where $\boldsymbol{\Gamma}$ is the matrix formed by $\Gamma_{ll'}(k_x,k_z)$ and

$$\mathbf{D}^<=\begin{pmatrix}\ddots & & \mathbf{0}\\ & d_l^< & \\ \mathbf{0} & & \ddots\end{pmatrix} \tag{3.25}$$

and $\mathbf{D}^>$ with the symbol $<$ changed by $>$ and

$$\boldsymbol{\alpha}^{\beta 0}=[\ \ldots,\alpha_{l-1}^{\beta 0},\alpha_l^{\beta 0},\alpha_{l+1}^{\beta 0},\ \ldots]^t,$$

$$\boldsymbol{\alpha}^{\beta<}=[\ \ldots,\alpha_{l-1}^{\beta<},\alpha_l^{\beta<},\alpha_{l+1}^{\beta<},\ \ldots]^t \tag{3.26}$$

define the column vectors $\boldsymbol{\alpha}^{\beta 0}$ and $\boldsymbol{\alpha}^{\beta<}$. By solving Eq. (3.24), we can obtain the unknown coefficient $\alpha_l^{\beta<}$ in terms of the initial data $\alpha_l^{\beta 0}$ of the incident light. To rewrite Eq. (3.24) more compactly, we introduce the matrices $\mathbf{D}_{\beta\beta'}^<$ and $\mathbf{D}_{\beta\beta'}^>$ through the transformation

$$\mathbf{D}_{\beta\beta'}^{<(>)}=\sum_j(\mathbf{P}_j^{\beta>})^\dagger\mathbf{D}^{<(>)}\mathbf{P}_j^{\beta'<} \tag{3.27}$$

and

$$\boldsymbol{\Gamma}_{\beta\beta'}=\sum_j(\mathbf{P}_j^{\beta>})^\dagger\boldsymbol{\Gamma}\mathbf{P}_j^{\beta'>}. \tag{3.28}$$

Their rows and columns are labeled by l as in Eq. (3.25). Then Eq. (3.24) is written as

$$\sum_{\beta'=M,N}(\mathbf{D}^<+\boldsymbol{\Gamma}\mathbf{D}^>)_{\beta\beta'}\boldsymbol{\alpha}^{\beta'<}=-\frac{2i}{\pi}\boldsymbol{\alpha}^{\beta 0} \tag{3.29}$$

with

$$(\boldsymbol{\Gamma}\mathbf{D}^>)_{\beta\beta'}=\sum_{\beta''=M,N}\boldsymbol{\Gamma}_{\beta\beta''}\mathbf{D}_{\beta''\beta'}^>. \tag{3.30}$$

To derive the right-hand side of Eq. (3.30), we have inserted the completeness relation Eq. (2.12) between $\boldsymbol{\Gamma}$ and $\mathbf{D}^>$ on the left-hand side. The contribution from the matrices $\mathbf{Q}_i$ of the completeness relation is shown to vanish, leaving behind only that from $\mathbf{P}^\beta(\mathbf{P}^\beta)^\dagger$ and hence leading to Eq. (3.30). The same situation happened in the case of arrayed spheres. See Ref. 25 for the proof of the vanishing of the $\mathbf{Q}_i$ contribution.

Equation (3.29) must be handled numerically. $\boldsymbol{\Gamma}_{\beta\beta'}$ is a function of the incident wave vectors k_x and k_z. It is worth pointing out that the quantities $\mathbf{D}^>$ and $\mathbf{D}^<$, or their matrix elements $d_l^>$ and $d_l^<$, as well as the scalar structure factor $\Gamma_{ll'}$ all appear without modification in the electron scattering. The vector version of the Maxwell fields is hence obtained simply by replacing them by those having the indices $\beta\beta'$, which are obtained by the simple transformations using $\mathbf{P}_i^\beta$. This is a key point of the conversion from the scalar to the vector treatment.[8] Since the indices $\beta\beta'$ define the 2×2 blocks, MM, MN, NM, and NN, Eq. (3.29) may be treated as a matrix equation of dimension twice as large as that of electrons. Therefore the good convergence experienced in the electronic case promises the same situation to arise in the photonic case.

Once Eq. (3.29) is solved, the inside field is given by Eq. (3.20). The field outside the cylinders is obtained from Eq. (3.14). Nearly the same calculation as above yields

$$\mathbf{E}_{k_x}^>(\mathbf{r})=\mathbf{E}_{k_x}^0(\mathbf{r})-\frac{i\pi}{2}\sum_{\beta\beta'}\sum_{ll'}\{\boldsymbol{\epsilon}_l^\beta(\mathbf{r};H(\lambda_>\rho))[\mathbf{D}_{\beta\beta'}^>]_{ll'}\alpha_{l'}^{\beta'<}$$
$$+\boldsymbol{\epsilon}_l^\beta(\mathbf{r};J(\lambda_>\rho))[(\boldsymbol{\Gamma}\mathbf{D}^>)_{\beta\beta'}]_{ll'}\alpha_{l'}^{\beta'<}\}. \tag{3.31}$$

In terms of this formula, we may approach an arbitrary point near the cylinder surface to obtain the near-field intensity.

To obtain the reflectivity or transmittivity of incident light, the expression (3.31) of the scattered field expressed in terms of the spherical waves is not convenient. For this purpose, the plane-wave amplitude of the scattered wave is necessary. Also, the plane-wave form of the scattered wave is important in the layer doubling method. To derive it, we substitute the following plane-wave form of the Green's function in Eq. (3.14) [for $\mathbf{E}^<(\mathbf{r}')$ of Eq. (3.15), we use the spherical-wave form]

$$g^{(0)}(\boldsymbol{\rho},\boldsymbol{\rho}')+g^{(1)}(\boldsymbol{\rho},\boldsymbol{\rho}')=\sum_h\frac{-i}{2d\gamma_h}e^{i(k_x+h)(x-x')+i\gamma_h|y-y'|}. \tag{3.32}$$

Here, in terms of the reciprocal lattice vector h in the x direction,

$$\gamma_h=[q^2-(k_x+h)^2-k_z^2]^{1/2} \tag{3.33}$$

defines the y component of the wave vector of the scattered lights, y being the direction perpendicular to the plane of the monolayer. By the diffraction, the scattered waves acquire the wave vector

$$\mathbf{k}_h^\pm=(k_x+h,\pm\gamma_h,k_z) \tag{3.34}$$

of various h with the label $+$ and $-$ for the propagating directions $+y$ and $-y$, respectively. When the channel h is

open, γ_h is real, showing that the $\mathbf{k}_{\mathbf{h}}^{\pm}$ waves are propagating, while they are evanescent for imaginary γ_h ($\mathrm{Im}\gamma_h>0$).

Now for the purpose of using them in the layer-doubling method, let us compile the scattering data from a monolayer in the xz plane. We assume that the incident field $\mathbf{E}^0(\mathbf{r})$ impinges upon the layer from the side $y<0$, i.e., $k_y>0$ in Eq. (3.9). We express the scattered light of the exterior of the monolayer as

$$\mathbf{E}_i^{>}(\mathbf{r})=\sum_h \sum_{i'} \exp(i\mathbf{k}_h^+\cdot\mathbf{r})[\mathbf{T}_{h0}^{++}]_{ii'}E_{i'}^0 \qquad (3.35)$$

for the wave with the wave vector $\mathbf{k}_h^+$ and

$$\mathbf{E}_i^{>}(\mathbf{r})=\sum_h \sum_{i'} \exp(i\mathbf{k}_h^-\cdot\mathbf{r})[\mathbf{R}_{h0}^{-+}]_{ii'}E_{i'}^0 \qquad (3.36)$$

for the wave backscattered with $\mathbf{k}_h^-$. The coefficients $\mathbf{T}$ and $\mathbf{R}$ are the amplitude transmission and reflection coefficients. The superscript of, e.g., $[\mathbf{R}_{h0}^{-+}]_{ii'}$ emphasizes the process of light in the $+y$ direction being reflected back in the $-y$ direction. The subscript $h0$ specifies the reciprocal lattice vectors of the wave vectors before and after the scattering. In parallel with the notation for the scattered wave vector, we use the notation $\mathbf{k}_0^+$ for the incident wave vector in the following formula. Then we find

$$[\mathbf{T}_{h0}^{++}]_{ii'}=\left(-\frac{i}{2d}\right)\frac{1}{\gamma_h}\mathbf{y}^t(\mathbf{k}_h^+)\boldsymbol{\tau}_{ii'}\mathbf{y}^*(\mathbf{k}_0^+)+\delta_{ii'}\delta_{h0},$$

$$[\mathbf{R}_{h0}^{-+}]_{ii'}=\left(-\frac{i}{2d}\right)\frac{1}{\gamma_h}\mathbf{y}^t(\mathbf{k}_h^-)\boldsymbol{\tau}_{ii'}\mathbf{y}^*(\mathbf{k}_0^+). \qquad (3.37)$$

The second term of $\mathbf{T}$ is the contribution of the incident light. Here $\mathbf{y}(\mathbf{k})$ is the column vector labeled by l,

$$\mathbf{y}(\mathbf{k})=[\ \ldots,e^{i(l-1)\theta(\mathbf{k})},e^{il\theta(\mathbf{k})},e^{i(l+1)\theta(\mathbf{k})},\ \ldots\ ]^t \qquad (3.38)$$

and

$$[\boldsymbol{\tau}_{ij}]_{ll'}=i^{-l+l'}\left[\sum_{\beta\beta'}\mathbf{P}_i^{\beta>}\boldsymbol{\tau}^{\beta\beta'}(\mathbf{P}_j^{\beta'>})^{\dagger}\right]_{ll'}, \qquad (3.39)$$

where

$$\boldsymbol{\tau}^{\beta\beta'}=\frac{4}{i}[\mathbf{D}^{>}(\mathbf{D}^{<}+\boldsymbol{\Gamma}\mathbf{D}^{>})^{-1}]_{\beta\beta'}. \qquad (3.40)$$

In addition to the transmission and reflection of the incident wave, we need to consider in the layer-doubling scheme the scattering of the waves with wave vector $\mathbf{k}_{h'}^{\pm}$. Its scattering data of $\mathbf{T}_{hh'}^{--}$ or $\mathbf{R}_{hh'}^{+-}$ are obtained from the above formula simply changing the wave vector 0 to h'. For example,

$$[\mathbf{R}_{hh'}^{+-}]_{ii'}=\left(-\frac{i}{2d}\right)\frac{1}{\gamma_h}\mathbf{y}^t(\mathbf{k}_h^+)\boldsymbol{\tau}_{ij}\mathbf{y}^*(\mathbf{k}_{h'}^-). \qquad (3.41)$$

When the vector $\mathbf{k}_{h'}$ is evanescent with imaginary k_y, $\mathbf{y}(\mathbf{k}_{h'})$ is real. In this case we must set

$$\mathbf{y}^*(\mathbf{k}_h^{\pm})=\mathbf{y}(\mathbf{k}_h^{\mp}) \qquad (3.42)$$

[see Eq. (2.16)].

This completes the monolayer scattering. Note that the plane-wave amplitudes of the scattered waves have the form expressed by the cylindrical waves. This should be so in order to make use of the first convergence. For numerical purpose there are two key points in programming these formulas. One is the matrix algebra involving the transformation matrices $\mathbf{P}_i^M$ and $\mathbf{P}_i^N$ and the other is to find out the formula guaranteeing the fast convergence of the scalar structure factor $\Gamma_{ll'}$. The latter is provided by the method used in band calculation of electrons and is described in Appendix A. In the rest of this section we deal with the former.

Simplifying the above formulae by using Eq. (2.9) is straightforward. For an arbitrary matrix $\mathbf{F}=(F_{ll'})$, it holds that $(u,v=>,<)$

$$\left\{\sum_j(\mathbf{P}_j^{\beta u})^{\dagger}\mathbf{F}\mathbf{P}_j^{\beta' v}\right\}_{ll'}$$

$$=\tfrac{1}{2}(F_{l+1,l'+1}+F_{l-1,l'-1}) \quad (\beta\beta')=(MM),$$

$$=\frac{1}{q_u q_v}\left[\frac{k_z^2}{2}(F_{l+1,l'+1}+F_{l-1,l'-1})\right.$$

$$\left.+\lambda_u\lambda_v F_{l,l'}\right] \quad (\beta\beta')=(NN),$$

$$=\frac{k_z}{2q_u}(-F_{l+1,l'+1}+F_{l-1,l'-1}) \quad (\beta\beta')=(MN),$$

$$=\frac{k_z}{2q_v}(-F_{l+1,l'+1}+F_{l-1,l'-1}) \quad (\beta\beta')=(NM), \qquad (3.43)$$

$q_>$ and $q_<$ being given by Eq. (3.17). To obtain the block matrices $\mathbf{D}_{MM}^{>}$, $\mathbf{D}_{MM}^{<}$, etc., defined by Eq. (3.27), $\mathbf{F}$ is playing the role of the diagonal matrix $\mathbf{D}^{>}$, $\mathbf{D}^{<}$, etc. From Eq. (3.43), we then find

$$(\mathbf{D}_{MM})_{ll'}=\delta_{ll'}\tfrac{1}{2}(d_{l+1}+d_{l-1}),$$

$$(\mathbf{D}_{MN})_{ll'}=\delta_{ll'}\frac{k_z}{2q_<}(-d_{l+1}+d_{l-1}),$$

$$(\mathbf{D}_{NM})_{ll'}=\delta_{ll'}\frac{k_z}{2q_>}(-d_{l+1}+d_{l-1}),$$

$$(\mathbf{D}_{NN})_{ll'}=\delta_{ll'}\left[\frac{k_z^2}{2q_>q_<}(d_{l+1}+d_{l-1})+\frac{\lambda_>\lambda_<}{q_>q_<}d_l\right]. \qquad (3.44)$$

The subscripts $<$ and $>$ must be supplied on both sides to obtain $\mathbf{D}^{<}$ and $\mathbf{D}^{>}$, respectively. By Eq. (3.44), they are thus diagonal with respect to l, l', with the quantities $d_l^{>}$ and $d_l^{<}$ given by Eq. (3.23).

For the structure factor $\boldsymbol{\Gamma}_{\beta\beta'}$, it is shown by Eq. (A13) that the scalar structure factor $\Gamma_{ll'}$ is the function of $l-l'$. Using this property in $\mathbf{F}$, we obtain

$$(\boldsymbol{\Gamma}_{MM})_{ll'}=\Gamma_{ll'},$$

$$(\mathbf{\Gamma}_{MN})_{ll'}=0,$$

$$(\mathbf{\Gamma}_{NM})_{ll'}=0,$$

$$(\mathbf{\Gamma}_{NN})_{ll'}=\Gamma_{ll'}. \tag{3.45}$$

It is interesting to note that the mixing via the structure factor between the M and N waves is absent and that the structure factors for M and N are the same as the scalar structure factor. The off-diagonal structure factor Γ_{NM} describes how much of the N wave is contained when the M-type wave, scattered out of the rods other than the r cylinder, is seen from the r cylinder. Since the M wave has vanishing z component [Eq. (2.4)], it continues to be a M wave irrespective of the observation point. This is the reason why $\mathbf{\Gamma}_{MN}=\mathbf{\Gamma}_{NM}=0$.

B. t matrix and scattering from a single cylinder

Before going on to the layer-doubling method, we comment on the light scattering from a single cylinder[26] and introduce the **t** matrix.

The formulas given in Sec. III A for the monolayer of scatterers cover the light scattering from a single dielectric rod, if we drop the terms involving the structure factor $\mathbf{\Gamma}$. To obtain the field expression outside the cylinder, we solve Eq. (3.29) for $\boldsymbol{\alpha}^{\beta'<}$ and substitute it into Eq. (3.31). Then we find the outside field expressed in terms of the initial amplitude $\boldsymbol{\alpha}^{\beta 0}$;

$$\mathbf{E}^{>}(\mathbf{r})=\mathbf{E}^{0}(\mathbf{r})-\sum_{\beta\beta'}\sum_{ll'}\boldsymbol{\epsilon}_{l}^{\beta}(\mathbf{r};H(\lambda_{>}\rho))[\mathbf{t}_{\beta\beta'}]_{ll'}\alpha_{l'}^{\beta' 0}. \tag{3.46}$$

The second term describing the outgoing scattered wave has the **t** matrix defined by

$$\mathbf{t}_{\beta\beta'}=\sum_{\beta''=M,N}\mathbf{D}^{>}{}_{\beta\beta''}[(\mathbf{D}^{<})^{-1}]_{\beta''\beta'}, \tag{3.47}$$

the second matrix being the $\beta''\beta'$ block of the inverse of the entire 2×2 matrix. The matrices $\mathbf{D}^{>}_{\beta\beta'}$ and $\mathbf{D}^{<}_{\beta\beta'}$ are both diagonal with respect to l [Eq. (3.44)] and so is the **t** matrix. However, Eq. (3.44) also shows that, when $k_z\neq 0$, the partial waves (M,l) and (N,l) mix due to the presence of the off-diagonal terms $\mathbf{D}^{>}_{MN}$ and $\mathbf{D}^{<}_{MN}$. Therefore, in the description of the light scattering from a cylinder we need in general four **t** matrices, $\mathbf{t}_{MM}$, $\mathbf{t}_{MN}$, etc. Setting

$$[\mathbf{D}^{>(<)}_{\beta\beta'}]_{ll'}=\delta_{ll'}d^{>(<)}_{\beta\beta'}(l), \tag{3.48}$$

we find

$$[\mathbf{t}_{\beta\beta'}]_{ll'}=\delta_{ll'}\left[\begin{pmatrix} d^{>}_{MM}(l) & d^{>}_{MN}(l)\\ d^{>}_{NM}(l) & d^{>}_{NN}(l)\end{pmatrix}\times\begin{pmatrix} d^{<}_{MM}(l) & d^{<}_{MN}(l)\\ d^{<}_{NM}(l) & d^{<}_{NN}(l)\end{pmatrix}^{-1}\right]_{\beta\beta'}. \tag{3.49}$$

In the light scattering from a sphere, the (M,l) and (N,l) partial waves do not mix,[8,25] leading to the two phase shifts δ_l^M and δ_l^N. In the cylindrical case of nonzero k_z, the two-phase shifts for an l are not obtained until after diagonalizing the 2×2 matrix of Eq. (3.49). To put it another way, the eigenphase shifts of the cylindrical case are neither purely of M nor of N, when $k_z\neq 0$.

Introducing the two phase shifts reduces various formulas, such as the total cross section of a single-cylinder scattering to compact forms, but in using the **t** matrix for the scattering from a collection of scatterers, the phase shifts are not very useful concepts, because after the diagonalization of the **t** matrix, the structure factor $\mathbf{\Gamma}_{\beta\beta'}$, diagonal with respect to $\beta\beta'$, is no longer diagonal.

Using the definition [Eq. (3.47)] of the **t** matrix, the formulas for the monolayer scattering given in Sec. III A are rewritten into more familiar forms. Equation (3.29), for example, is transformed to

$$\sum_{\beta'\beta''}(\mathbf{t}^{-1})_{\beta\beta'}(\mathbf{I}+\mathbf{t}\mathbf{\Gamma})_{\beta'\beta''}\boldsymbol{\alpha}^{\beta''<}=-\frac{2i}{\pi}\boldsymbol{\alpha}^{\beta 0}. \tag{3.50}$$

Using this, the quantity $\mathbf{D}^{>}_{\beta\beta'}\boldsymbol{\alpha}^{\beta'<}$ of Eq. (3.31) transforms into

$$\mathbf{D}^{>}_{\beta\beta'}\boldsymbol{\alpha}^{\beta'<}=[(\mathbf{I}+\mathbf{t}\mathbf{\Gamma})^{-1}\mathbf{t}]_{\beta\beta'}\alpha^{\beta' 0}, \tag{3.51}$$

$\mathbf{I}$ being the unit matrix $(\mathbf{I})_{\beta\beta',ll'}=\delta_{\beta\beta'}\delta_{ll'}$. In this way all the formulas of the monolayer scattering may be reexpressed in terms of the **t** matrix of the one-cylinder scattering and the structure factor. The inverse matrix $(\mathbf{I}+\mathbf{t}\mathbf{\Gamma})^{-1}$, when expanded as a power series with respect to $\mathbf{t}\mathbf{\Gamma}$, implies that the monolayer scattering is nothing but the infinite sequence of the scattering by individual cylinders followed by the propagation between the cylinders.

C. Layer-doubling method

It was shown[9] that the iteration method of taking into account the successive scatterings from the stacking layers breaks down in the frequency range of the heavy photons. The layer-doubling method, which treats the scattering between the two neighboring layers exactly, remedies this. Since the detailed description of it is found in the articles for low-energy electron diffraction (LEED) of Pendry[27] and Tong[28] and the works on photonic bands of Pendry[29] and of Ohtaka and Tanabe,[9] we are giving without derivation a series of necessary formulas, after giving a brief review of its content.

Now let us consider a plane-wave light incident upon the system composed of two parallel layers A and B (the layer A is above B). The waves outside the layers, propagating or evanescent, may be expressed by the plane waves with wave vector $\mathbf{k}_h^{\pm}$. Assume a $\mathbf{k}_{h'}^{+}$ wave of unit amplitude propagating upwards between the two layers. When it passes through layer A, a set of transmitted waves of wave vectors $\mathbf{k}_h^{+}$, with various h, come out with amplitude $\mathbf{T}^{++}_{hh'}$. At the same time layer A gives rise to the diffracted waves of wave vectors $\mathbf{k}_h^{-}$ back to B with amplitudes $\mathbf{R}^{-+}_{hh'}$. At layer B these reflected waves are diffracted, each giving birth to a set of transmitted and reflected waves with the additional factors $\mathbf{T}^{--}$ and $\mathbf{R}^{+-}$, respectively. The infinite repetition of this process occurs and the transmission coefficient in the upward direction for the combined system of AB is obtained by the sum of the

contributions of all turns. It is indeed incorporated by the inverse matrix $[\mathbf{I}-\mathbf{R}^{++}\mathbf{R}^{-+}]^{-1}$, where the index h for the wave vector and i for the polarization component label the scattering matrices and $\mathbf{I}$ is the unit matrix $\mathbf{I}=(\delta_{ii'}\delta_{hh'})$. A minor complication occurs due to the phase difference between the two layers, which is incorporated by redefining the scattering data with a phase factor. Once the scattering data for the combined two layers are obtained, they are used to construct the data for the combined four layers. The nth run gives the transmission and reflection coefficients for the 2^n layers.

Setting as subscripts A and B for the scattering matrices of the two layers (we do not need them when the two are identical), the $\mathbf{T}$ and $\mathbf{R}$ matrices for the combined system, called C, is obtained as

$$\begin{aligned}\tilde{\mathbf{T}}_C^{++}&=\tilde{\mathbf{T}}_B^{++}\tilde{\mathbf{T}}_A^{++}+\tilde{\mathbf{T}}_B^{++}\tilde{\mathbf{T}}_B^{++}\tilde{\mathbf{R}}_A^{+-}\tilde{\mathbf{R}}_B^{-+}\tilde{\mathbf{T}}_A^{++}\\&\quad+\tilde{\mathbf{T}}_B^{++}(\tilde{\mathbf{R}}_A^{+-}\tilde{\mathbf{R}}_B^{-+})^2\tilde{\mathbf{T}}_A^{++}+\cdots\\&=\tilde{\mathbf{T}}_B^{++}[1-\tilde{\mathbf{R}}_A^{+-}\tilde{\mathbf{R}}_B^{-+}]^{-1}\tilde{\mathbf{T}}_A^{++},\\ \tilde{\mathbf{T}}_C^{--}&=\tilde{\mathbf{T}}_A^{--}[1-\tilde{\mathbf{R}}_B^{-+}\tilde{\mathbf{R}}_A^{+-}]^{-1}\tilde{\mathbf{T}}_B^{--},\\ \tilde{\mathbf{R}}_C^{-+}&=\tilde{\mathbf{R}}_A^{-+}+\tilde{\mathbf{T}}_A^{--}\tilde{\mathbf{R}}_B^{-+}(1-\tilde{\mathbf{R}}_A^{+-}\tilde{\mathbf{R}}_B^{-+})^{-1}\tilde{\mathbf{T}}_A^{++},\\ \tilde{\mathbf{R}}_C^{+-}&=\tilde{\mathbf{R}}_A^{+-}+\tilde{\mathbf{T}}_B^{++}\tilde{\mathbf{R}}_A^{+-}(1-\tilde{\mathbf{R}}_B^{-+}\tilde{\mathbf{R}}_A^{+-})^{-1}\tilde{\mathbf{T}}_B^{--},\end{aligned}\tag{3.52}$$

with

$$\begin{aligned}\tilde{\mathbf{T}}_{hh'}^{\pm\pm}&=\exp\left(\pm i\mathbf{k}_h^{\pm}\cdot\frac{\mathbf{t}}{2}\right)\mathbf{T}_{hh'}^{\pm\pm}\exp\left(\pm i\mathbf{k}_{h'}^{\pm}\cdot\frac{\mathbf{t}}{2}\right),\\ \tilde{\mathbf{R}}_{hh'}^{\pm\mp}&=\exp\left(\pm i\mathbf{k}_h^{\pm}\cdot\frac{\mathbf{t}}{2}\right)\mathbf{R}_{hh'}^{\pm\mp}\exp\left(\pm i\mathbf{k}_{h'}^{\mp}\cdot\frac{\mathbf{t}}{2}\right).\end{aligned}\tag{3.53}$$

Here the vector $\mathbf{t}=(t_x,t_y)$ is equal to $\mathbf{r}_B-\mathbf{r}_A$, $\mathbf{r}_A$ and $\mathbf{r}_B$ being the 2D vector for the center positions of the r cylinders of the two layers. The r cylinder may be chosen to be any one of the rods of each layer. Note that the phase factors in Eq. (3.53) need to be added solely in the first run. In constructing the data for four layers, for example, the data obtained in the first run are used as they are on the right-hand side of Eq. (3.52).

D. Secular equation for the band structure

In Sec. III A we treated a single plane of arrayed rods. Band calculation is carried out for the infinite array of rods but its formulation does not require any additional task.

If there is no incident wave, the right-hand side of Eq. (3.29) is zero:

$$\sum_{\beta'}[\mathbf{D}^{<}+\mathbf{\Gamma}\mathbf{D}^{>}]_{\beta\beta'}\boldsymbol{\alpha}^{\beta'<}=0.\tag{3.54}$$

Explicitly,

$$\left[\begin{pmatrix}\mathbf{D}_{MM}^{<}&\mathbf{D}_{MN}^{<}\\ \mathbf{D}_{NM}^{<}&\mathbf{D}_{NN}^{<}\end{pmatrix}+\begin{pmatrix}\mathbf{\Gamma}_{MM}&0\\0&\mathbf{\Gamma}_{NN}\end{pmatrix}\begin{pmatrix}\mathbf{D}_{MM}^{>}&\mathbf{D}_{MN}^{>}\\ \mathbf{D}_{NM}^{>}&\mathbf{D}_{NN}^{>}\end{pmatrix}\right]\times\begin{pmatrix}\boldsymbol{\alpha}^{M<}\\ \boldsymbol{\alpha}^{N<}\end{pmatrix}=0,\tag{3.55}$$

where we have used Eq. (3.45). This equation determines the normal modes of the monolayer of 2D wave vector (k_x,k_z). Thus the eigenvalues are given by the zeros of the secular determinant formed from the coefficients (they are, however, complex in the monolayer case because of the radiation damping, as in the Mie resonance of a single-sphere case):

$$\det\left[\begin{pmatrix}\mathbf{D}_{MM}^{<}&\mathbf{D}_{MN}^{<}\\ \mathbf{D}_{NM}^{<}&\mathbf{D}_{NN}^{<}\end{pmatrix}+\begin{pmatrix}\mathbf{\Gamma}_{MM}&0\\0&\mathbf{\Gamma}_{NN}\end{pmatrix}\begin{pmatrix}\mathbf{D}_{MM}^{>}&\mathbf{D}_{MN}^{>}\\ \mathbf{D}_{NM}^{>}&\mathbf{D}_{NN}^{>}\end{pmatrix}\right]=0.\tag{3.56}$$

The eigenvectors $\boldsymbol{\alpha}^{\beta<}$ determine the electric field of the eigenmode through Eq. (3.20) in the inside region and the outside field is determined through Eq. (3.31), with the incident field $\mathbf{E}_{k_x}^0(\mathbf{r})$ dropped. Namely,

$$\mathbf{E}^{<}(\mathbf{r})=\sum_{\beta}\sum_{l}\boldsymbol{\epsilon}_l^{\beta}(\mathbf{r};J(\lambda_{<}\rho))\alpha_l^{\beta'<}\tag{3.57}$$

for $\mathbf{r}$ inside the r cylinder and

$$\begin{aligned}\mathbf{E}^{>}(\mathbf{r})=-\frac{i\pi}{2}\Bigg[&\sum_{\beta,\beta'}\sum_{l,l'}\boldsymbol{\epsilon}_l^{\beta}(\mathbf{r};H(\lambda_{>}\rho))[D_{\beta\beta'}^{>}]_{ll'}\alpha_l^{\beta'<}\\&+\sum_{\beta,\beta'}\sum_{l,l'}\boldsymbol{\epsilon}_l^{\beta}(\mathbf{r};J(\lambda_{>}\rho))[(\Gamma D^{>})_{\beta\beta'}]_{ll'}\alpha_{l'}^{\beta'<}\Bigg]\end{aligned}\tag{3.58}$$

for $\mathbf{r}$ outside.

So far we have considered a monolayer system. To obtain the secular equation for an infinite 3D array of cylinders, we note that, as shown at the end of Sec. III B, Eq. (3.56) is equivalent to the equation $\det[\mathbf{I}+\mathbf{t}\mathbf{\Gamma}]=0$ with the 2×2 block matrices $\mathbf{\Gamma}$ [Eq. (3.28)] and $\mathbf{t}$ [Eq. (3.47)] for the structure factor and the $\mathbf{t}$ matrix, respectively. We also mentioned that the inverse matrix $[\mathbf{1}+\mathbf{t}\mathbf{\Gamma}]^{-1}$, whose poles are given by the zeros of Eq. (3.56), describes a sequence of scattering in the lattice of cylinders. The combination of the $\mathbf{t}$ matrix with the structure factor is a general form of the scattering, valid for any collection of (nonoverlapping) scatterers, not restricted to the scattering from a monolayer.[25] How the scatterers are distributed is completely determined by the structure factor. See, e.g., Eq. (28) of Felbacq and Maystre for the light scattering from a group of cylinders[30] and Eq. (2.13) of Ohtaka and Inoue for a group of spheres.[31] Thus an infinite 3D array of cylinders is treated by quite the same equations as appeared in the monolayer scattering, if only we take account of the change of lattice in the structure factor.

The scalar structure factor $\Gamma(\mathbf{k})_{ll'}$ is now dependent upon the 3D wave vector $\mathbf{k}$ of the Bloch wave. From it, the conversion to the vector version is carried out through Eq. (3.28) and we find, just as in Eq. (3.45), that $\mathbf{\Gamma}_{MM}(\mathbf{k})$ and $\mathbf{\Gamma}_{NN}(\mathbf{k})$ are both equal to the scalar structure factor. The conclusion is thus that the set of Eqs. (3.55)–(3.58) are all valid for the

band calculation of an infinite 3D system, if we use an appropriate scalar structure factor.

The remaining task is to give the expression of $\Gamma_{ll'}$ for the array of the cylindrical rods. For 3D lattices of atoms or spheres, the expressions are given by Kambe[32] and Ham and Segall[33] and have been widely used in electronic band-structure calculations and photonic bands.[8] In the present problem the array of the parallel rods introduces a 1D periodicity of spacing d in the monolayer case and a 2D periodicity in the band calculation. Although the modification is straightforward, still, a lot of calculations are necessary to arrive at the final results. Thus the list of them seems useful and we give it in Appendixes B and C.

IV. CONVERGENCE OF PLANE-WAVE EXPANSION

In this section we examine the convergence of the plane-wave method of band calculation. This topic is examined extensively by Haus and collaborators by seeing how the plane-wave results change with increasing number of plane waves.[22,34] As these authors emphasized, a comparison with the exact band energies is essential, because the convergence was found to be very slow.

There are two plane-wave calculation methods widely employed in the literature. Let us call them E and H methods following Haus and co-workers. The E method is used to solve Maxwell's equation,

$$\nabla\times\nabla\times\mathbf{E}_{n,\mathbf{k}}(\mathbf{r})-\omega^2\varepsilon(\mathbf{r})\mathbf{E}_{n,\mathbf{k}}(\mathbf{r})=0, \tag{4.1}$$

using the plane-wave form of the Bloch wave of band index n and wave vector $\mathbf{k}$,

$$\mathbf{E}_{n,\mathbf{k}}(\mathbf{r})=\sum_{\mathbf{h}}\mathbf{E}_{n,\mathbf{k}}(\mathbf{h})\exp[i(\mathbf{k}+\mathbf{h})\cdot\mathbf{r}]. \tag{4.2}$$

Here $\mathbf{k}=(k_x,k_y,k_z)$ is a 3D wave vector and $\mathbf{h}$ is a 2D reciprocal lattice vector in the xy plane, with the z direction chosen parallel to the axis of rods. The secular equation of the E method is[35]

$$\det|[(\mathbf{k}+\mathbf{h})^2\delta_{ij}-(\mathbf{k}+\mathbf{h})_i(\mathbf{k}+\mathbf{h})_j]\delta_{\mathbf{hh}'}-\omega^2\varepsilon_{\mathbf{hh}'}\delta_{ij}|=0, \tag{4.3}$$

with $\varepsilon_{\mathbf{hh}'}$ the $\mathbf{h}-\mathbf{h}'$ Fourier component of $\varepsilon(\mathbf{r})$ and i the three Cartesian components $(i=1,2,3)$. Since $(\mathbf{h},i)$ labels the rows and columns of the matrix, the dimension of the secular matrix is $3N\times 3N$, N being the number of the reciprocal lattice points considered.

The second is the H method for the magnetic field $\mathbf{H}_{n,\mathbf{k}}(\mathbf{r})$, which satisfies Maxwell's equation

$$\nabla\times\{\varepsilon^{-1}(\mathbf{r})\nabla\times\mathbf{H}_{n,\mathbf{k}}(\mathbf{r})\}-\omega^2\mathbf{H}_{n,\mathbf{k}}(\mathbf{r})=0. \tag{4.4}$$

With the Bloch magnetic-field expanded in the same way as above, the secular equation is obtained as[36]

$$\det|(\mathbf{k}+\mathbf{h})\cdot(\mathbf{k}+\mathbf{h}')\varepsilon^{-1}_{\mathbf{hh}'}\delta_{ij}-(\mathbf{k}+\mathbf{h})_j\varepsilon^{-1}_{\mathbf{hh}'}(\mathbf{k}+\mathbf{h}')_i-\omega^2\delta_{\mathbf{hh}'}\delta_{ij}|=0, \tag{4.5}$$

with $\varepsilon^{-1}_{\mathbf{hh}'}$ the Fourier component of $\varepsilon(\mathbf{r})^{-1}$.

For concreteness we consider the square lattice of rods with two basis vectors of the unit cell chosen in the x and y directions. For the special case of a wave vector of vanishing k_z, which we are examining here, the bands are classified into two groups. The one is composed of TE bands, having the eigenvector $\mathbf{E}_{n,\mathbf{k}}(\mathbf{h})$ of Eq. (4.2) in the xy plane for all $\mathbf{h}$. The eigenvector $\mathbf{H}_{n,\mathbf{k}}(\mathbf{h})$ is pointed in the z direction. The other is the TM group with $\mathbf{E}_{n,\mathbf{k}}(\mathbf{h})$ in the z direction and $\mathbf{H}_{n,\mathbf{k}}(\mathbf{h})$ in the xy plane.

We denote the bands of TE and TM characters by the symbols Exy and Ez, respectively, the subscript xy or z standing for the polarization direction of $\mathbf{E}_{n,\mathbf{k}}(\mathbf{h})$. For the Exy bands, the E method deals with a $2N\times 2N$ matrix in the secular equation, while the H method solves an $N\times N$. For the Ez bands, the dimension is reversed in the two methods.

Hereafter we examine the band energies for $\mathbf{k}=(0,k_y,0)$, i.e., for the wave vector along the Γ-X axis of the Brillouin zone. The band energies of the cylindrical-wave expansion are obtained by solving Eq. (3.56), with Eqs. (3.45), (A14), and (B1) taken into account. The calculation is made for the three cases of $\varepsilon_<=2$, $\varepsilon_<=4$, and $\varepsilon_<=3.2^2$. For the value of 3.2, see the comment given in Sec. V. These values are chosen arbitrarily as representatives of small, intermediate, and large dielectric constants. The radius a of the rod is taken to be 0.3 times the lattice constant d. For all the cases examined below, the cylindrical-wave formalism is found to converge when the partial waves of $l\leqslant 6$ are included. Thus the band energies thereof, referred to as exact band energies in what follows, are obtained from the 26×26 secular matrices. [Strictly speaking, the M and N blocks of Eq. (3.56) decouple in the present case of $k_z=0$, so that the Exy band energies are obtained from the 13×13 M block and the Ez band energies from the 13×13 N block.]

The band structure of the cylindrical-wave formalism is given for $\mathbf{k}=(0,k_y,0)$ in Fig. 1 for the three values of $\varepsilon_<$. The horizontal axis is the wave number k_y normalized by $2\pi/d$, with the Brillouin-zone boundary (X point) at $k_y=0.5$. The quantity Z in the vertical axis is the dimensionless frequency normalized by $2\pi/d$ $(c=1)$. In this scale, the dispersion relation of photons in free space is $Z=k_y$. In (d) the band structure for $\varepsilon_<=3.2^2$ of the region $Z>1$ is shown to give an image of how the band population becomes dense with increasing Z and $\varepsilon_<$. Several frequencies marked in Fig. 1 are the exact values to be cited below.

Now let us see how the solutions of Eqs. (4.3) and (4.5) change with increasing N. Figure 2 shows the typical results of the E and H methods, (a) for Exy and (b) for Ez bands of the intermediate case of $\varepsilon_<=4$ with $k_y=0.3$, whose exact values are marked in Fig. 1(b). The filled (open) circles are the results of the E (H) method with the straight line showing the exact value of Fig. 1(b). The arrow marks the frequency range of $\pm 1\%$ of the exact value.

In Fig. 2(a) we see that the values of the two methods converge correctly to the exact value with increasing N, though the convergence is very slow. Two things are to be noted: one is that the exact band energy is sandwiched by the E and H methods. This is a feature observed in all the cases examined in the present work. Thus one can conclude that the exact band energies are generally estimated by the combined use of E and H methods. The other is that the result of the H method is much worse than that of the E. This is already remarked by the works of Haus and co-workers.[34]

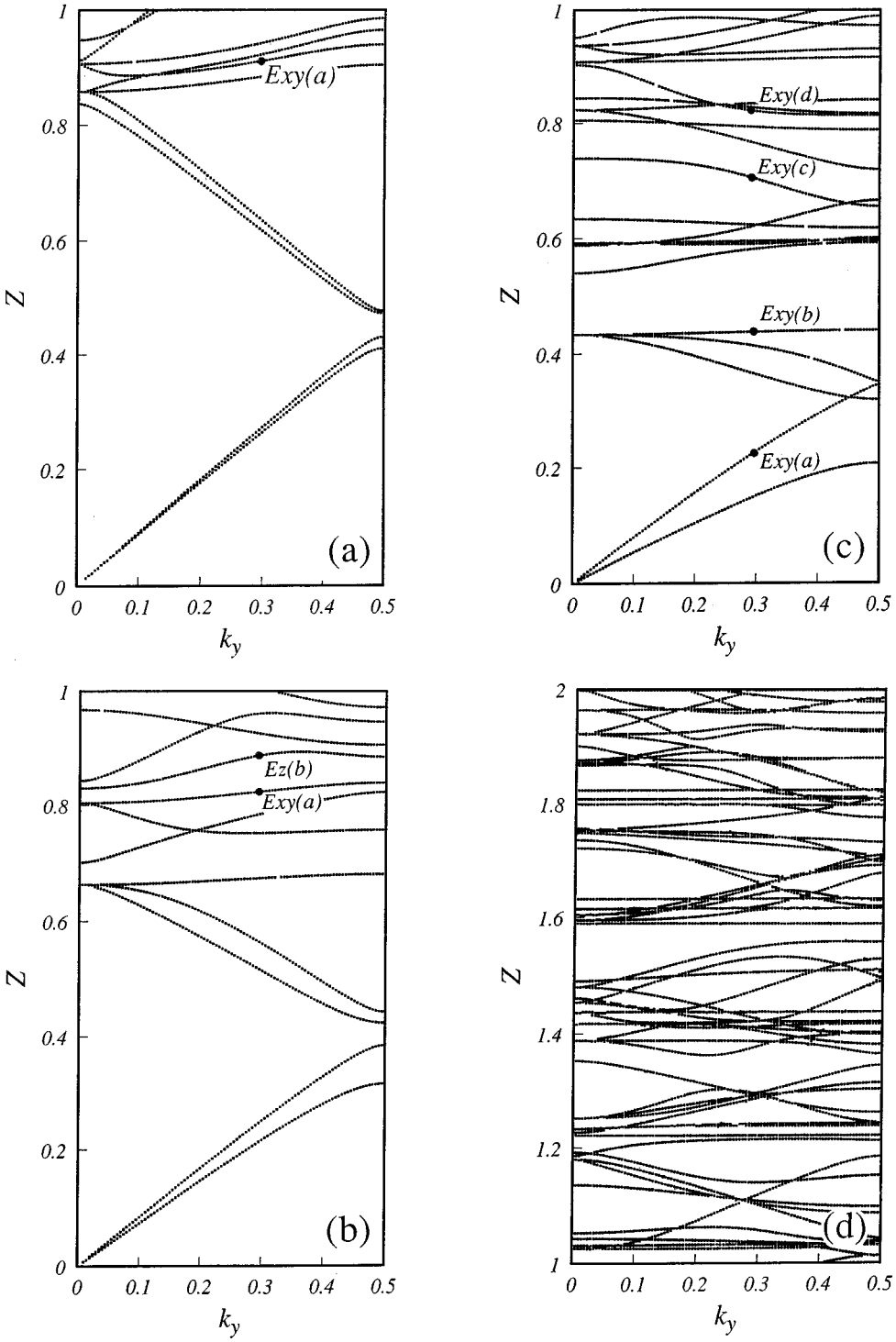

FIG. 1. Band structure between Γ and X points [$\mathbf{k}=(0,k_y,0)$] for three values of dielectric constant $\varepsilon_<$; (a) for $\varepsilon_<=2$, (b) for $\varepsilon_<=4$, and (c) and (d) for $\varepsilon_<=10.24$. The marked band energies at $k_y=0.3$ are investigated in Figs. 2, 3, and 4 and referred to as exact band energies.

Therefore, the H method, which treats the Exy bands by the scalar equation, does not profit. This second feature is not always the case, however, as shown by some exceptions below.

In Fig. 2(b), we plot the result of the E method. A remarkably good convergence is observed for the Ez band. We confirmed that this feature is generally the case. The conclusion is thus that, roughly speaking, a common N assures for Ez bands an accuracy of one more significant figure than for Exy bands. Since the E method works already quite well, we need not rely upon the H method for Ez bands, which solves a secular matrix twice as large. This is why the H-method calculation is not made in Fig. 2(b).

We hereafter confine ourselves to the Exy bands. Let us next see the dependence on the magnitude of $\varepsilon_<$. Figure 3 shows the convergence for the case of $\varepsilon_<=2$, the arrows marking in this case the range of $\pm 0.1\%$ of the exact band energy. One of the exact values shown by the straight lines is

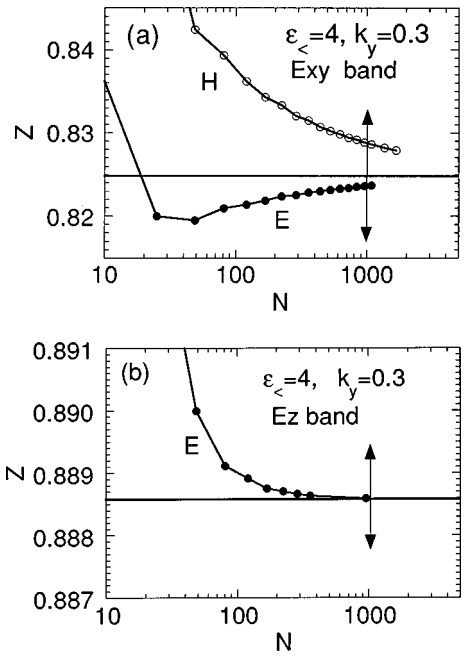

FIG. 2. Band energies of the E and H methods vs N; the panel (a) for the Exy band and (b) for the Ez bands, of $k_y=0.3$ and $\varepsilon_<=4$. In (a) the filled (open) circles show the result of E method (H method). In (b) only the result of the E method is shown. The straight lines show the exact band energies of Fig. 1(b), marked there as Exy(a) and Ez(b). The arrow shows the range of $\pm 1\%$ of the exact value.

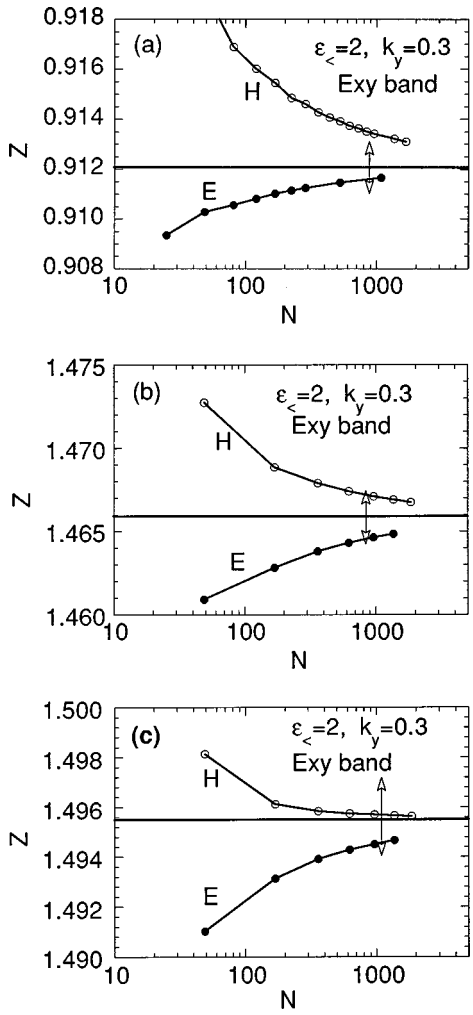

FIG. 3. Convergence of the band energies of the E and H methods for $\varepsilon_<=2$ and $k_y=0.3$. (a)–(c) treat the bands of relatively high frequency. The straight lines show the exact band energies. The exact value of (a) is shown in Fig. 1(a) as Exy(a). The arrow shows the range of the relative error of 0.1% above and below the exact value.

marked in Fig. 1(a). We see that in the case of the small dielectric constant of $\varepsilon_<=2$, one can obtain with $N=1000$ very good band energies lying within the error range of 0.1%, in the whole range of $0<Z<1.5$. It is remarkable that taking $N=100$ already assures band energies with the errors less than 1%. In part (b) the H method yields slightly better results than the E method. This is an exceptional case as stated above.

Figure 4 shows the case of the large dielectric constant of $\varepsilon_<=3.2^2$. (a) and (b) show the band energies of $Z\ll 1$ and (c) and (d) those of $Z\simeq 1$. (f) examines the band energy very near the zone boundary. The arrows show the error range of $\pm 1\%$ above and below the exact band energy. By comparing with Figs. 2 and 3, we see that the larger the magnitude of $\varepsilon_<$ is, the worse becomes the convergence. This feature of course reflects the enhanced localization of heavy photons with increasing dielectric constant. We note that in order to obtain the precision with the error less than 1% in the range of $0<Z<1.5$, we must set $N=1000$ for the case $\varepsilon_<\simeq 10$. The number 1000 should be compared with the number 13, stated above, of the dimension needed for the convergence of the cylindrical-wave calculation. We should say that it is hardly possible for the plane-wave methods to yield the precision of three decimal places for the case of $\varepsilon_<\simeq 10$, except for the band energies of $Z\ll 1$. We also note that in (a) the H method behaves much better than the E method. This case provides another example, for claiming that in the plane-wave calculation we had better use both the E and H methods, because they work complementarily. In (e) we can confirm that the zone boundary has no special effect on the convergence.

To make a detailed comparison of some data with the band scheme in the frequency range $Z>1$, precision with an error less than 0.1% is sometimes required. One of the examples will be found in Sec. V, where we see the transmittivity of light in relation to the band scheme. Generally speaking, however, an error of 0.1% is too stringent. For example, numerical searches for the possibility of a complete band gap have usually been carried out with respect to the first or second gap.[37] In these cases, a sufficiently reliable conclusion may be deduced from the band calculation with the errors on the order of, or even larger than, 1%. It is, however, important to note that a finite truncation of the plane-wave series fails to reproduce the precise profile of the dielectric function near the surface of rods. When we speak about the field intensity set up near the surface of rods, therefore, we must be very careful in applying the plane-wave calculation even if it works satisfactorily as regards the band energies.

To summarize, as long as the bands of the wave vector with $k_z=0$ and the dielectric rods with $\varepsilon_<\simeq 2$ are concerned, the E method assures the band scheme within the error of

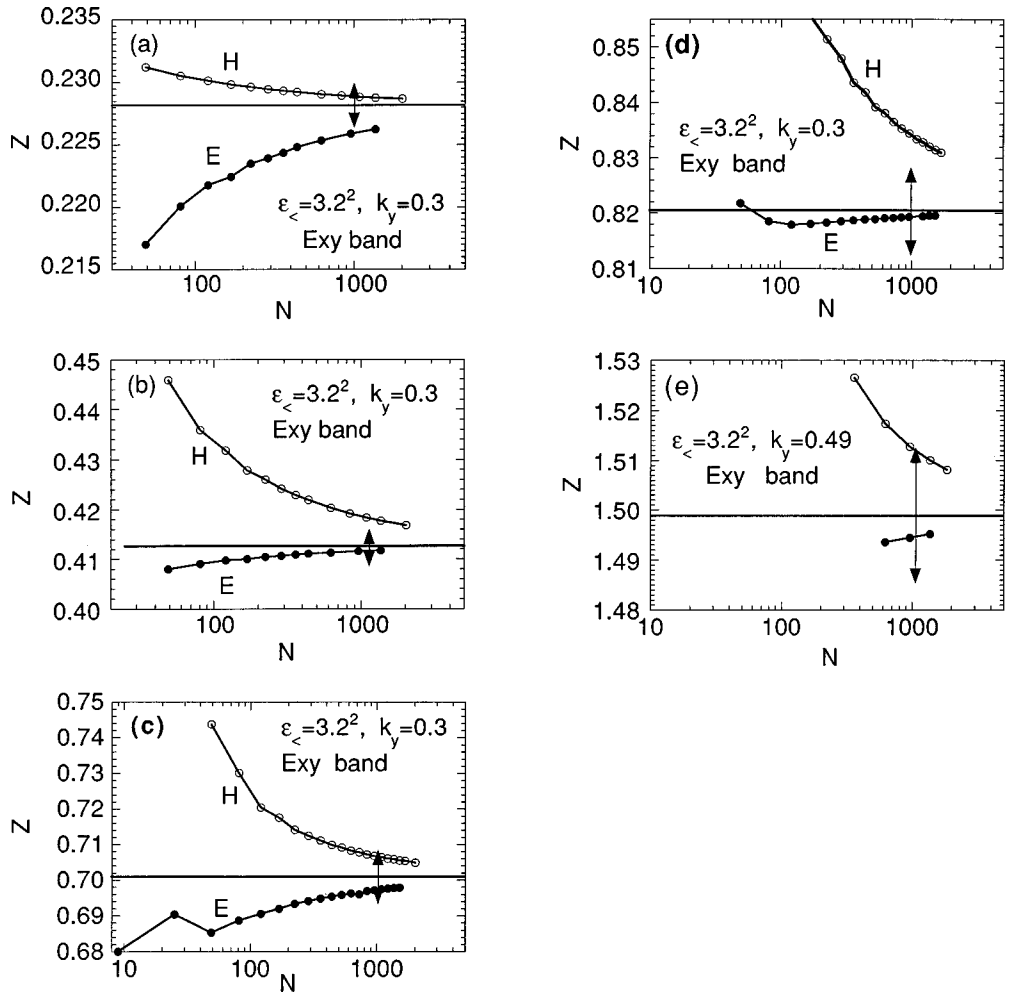

FIG. 4. Convergence of the E and H methods for the case of $\varepsilon_<=10.24$. The arrow shows the range of $\pm 1\%$ of each of the exact values shown by the straight lines. The exact values in (a)–(d) are marked in Fig. 1(c) as Exy(a)–Exy(d), respectively. (e) examines the state near the X point.

1% in the range $0<Z<1.5$, if we take $N\simeq 100$. In the case of $\varepsilon_<\simeq 10$, we need $N\simeq 1000$ to obtain the same accuracy in the range of $0<Z<1.5$, i.e., we must treat a 2000×2000 secular matrix in the E method. For the case of $\varepsilon_<\simeq 2$, the number $N=1000$ of the plane waves assures very good results of the relative error of 0.1% throughout the frequency range $Z<1.5$. Precision with an error of 0.1% is very hard to obtain in the plane-wave method in the case of $\varepsilon_<\simeq 10$, unless Z is much less than 1.0. In the higher-frequency range of $Z\gg 1$, the bands are more and more densely populated as inferred from Fig. 1(d). The precision of three decimal places of the band energies is crucial to arrive at a correct band ordering, because the magnitude of the error depends on bands.

For the band calculation for the wave vector $k_z\neq 0$, the dimension of the matrices is three times N in both E and H methods, so that the case of a large dielectric constant is very time consuming. It is to be noted that even for such general $\mathbf{k}$ the dimension of the cylindrical-wave secular matrix is still 26×26 for the bands with $Z\leqslant 1.5$.

Finally, the general aspect of the H method being worse than the E method results from the derivative involved in the first $\nabla\times$ of Eq. (4.4), which operates on $1/\varepsilon(\mathbf{r})$, producing a δ function singularity on the surface of rods, where $\varepsilon(\mathbf{r})$ has a step change. The Fourier transform in the H method is thus more slowly convergent than the E method.

V. EXAMPLES OF BAND AND TRANSMITTIVITY CALCULATIONS

We go on to present some of the numerical applications of our formalism. Since the band calculation involving a very large l and for the wave vector $\mathbf{k}$ with $k_z\neq 0$ is planned to be given in the following papers, we restrict ourselves in this paper to the case of $k_z=0$ and to the modest magnitudes of the value of l, as examined in Sec. IV. As the band and transmittivity calculations for $k_z=0$ are carried out and discussed by many authors,[1,2,38–42] our results will be given without a detailed discussion. But we choose the topic that needs the precision of data beyond the reach of the plane-wave method.

The system we examine here is the same as that of Sec. IV. In the band calculation a square lattice of cylinders of $\varepsilon_<=3.2^2$ is considered. The value 3.2 is twice the index of refraction of a polystyrene sphere in the visible range. The cylinder axis is in the z direction and two basis vectors of unit cell are in the x and y directions. When applying the layer doubling method, the y axis will be chosen to be the

thickness direction of the stacking 2D planes of rods. We take the radius a of the cylinder to be $0.3d$, d being the square size. We show the results in terms of the dimensionless frequency Z and wave number k introduced in Sec. IV.

If we wish to obtain for $\varepsilon_< = 3.2^2$ the reliable data within an error of 0.1%, the practical frequency range of the E method of $N = 1000$ must be limited to the range $Z \ll 1.0$, as shown in Sec. IV. Also, the transmittivity calculation by superposing the plane waves is limited to a small number $\Lambda \simeq 10$ of the stacking planes.[43] The cylindrical-wave results given below are for the frequency range $0 < Z < 2.0$ and $\Lambda = 32$. Actually, we calculated transmittivity for the system with $\Lambda = 256$, but the results do not differ very much from the result shown below except for the interference fringes. In the cylindrical-wave calculation the convergence is assured if we include $|l| < 7$ for $0 < Z < 2.0$. Also, in the layer-doubling method, about 100 reciprocal lattice points are enough for the matrices $\tilde{\mathbf{R}}$ or $\tilde{\mathbf{T}}$, introduced in Eq. (3.50).

Figure 5 shows the transmission coefficient of a plane-wave light polarized in the z direction. The horizontal axis shows $T(32)$, the transmittivity $|[T_{00}^{++}]_{zz}|^2$ for $\Lambda = 32$, and the vertical axis is the frequency Z. In the region of stop bands, $T(32)$ is zero and the incident light is totally reflected at the entrance surface. To see the relation between the transmittivity and the band structure, we superimpose in Fig. 5 the results of Figs. 1(c) and 1(d), as a function of k_y shown in the upper horizontal axis. (a) is for the region $0 < Z < 1.0$ and (b) for $1.0 < Z < 2.0$. Due to the translational invariance in the xz plane, the bands excited inside by the external light of normal incidence have a wave vector of $k_x = k_z = 0$. So that the relevant bands to consider here in relation to the transmittivity are only those of $\mathbf{k} = (0, k_y, 0)$. The value of k_y of the excited wave may be determined by cutting the dispersion curves by the horizontal line at the excitation frequency.

The presence of several stop bands and the clear interference fringes between them are the two striking features of the transmittivity. Although the Λ dependence of $T(\Lambda)$ is not given here, one of the interference fringes is suppressed markedly with increasing Λ and finally develops to a complete stop band. For the complete formation the lowest stop band needs $\Lambda = 16$, but mostly $\Lambda = 4$ or 8 is already enough. The oscillation in Z between two neighboring stop bands becomes gradually rapid with Λ, reflecting the phase $\exp(i\Lambda k_y)$, k_y being the wave-vector component of the excited wave. At $\Lambda = 32$, a detailed comparison of the positions of the stop bands with the band scheme for $\Lambda = \infty$ becomes possible. In the range of $Z < 1$, where the band population is relatively sparse, we can observe a clear correspondence between the stop bands and band edges. The bands sandwiched between the stop bands are those of heavy photons with small dispersion relation of the type $Z = \alpha + \beta k^2$. The clear interference fringes of $T(32)$ are obviously a proof for the good coherence of the heavy photons, in spite of their finite ''mass'' α and very slow group velocity attributable to very small β. In (b), the comparison between $T(32)$ and the band structure is rather difficult because of the enhanced density of bands.

The transmittivity of the x-polarized light presents analogous features, though the position of the stop bands has nothing to do with that of the z-polarized light shown in Fig. 5.

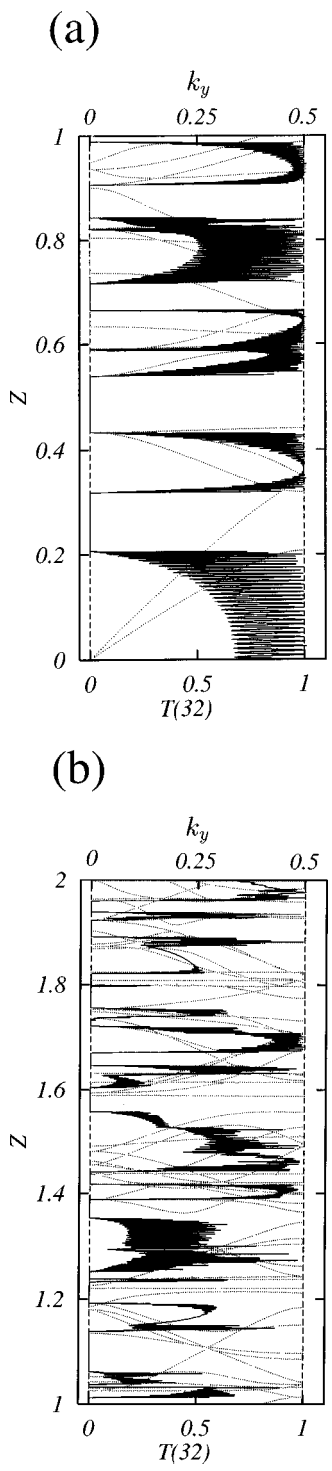

FIG. 5. Transmittivity of a z-polarized light of normal incidence as a function of frequency. The vertical axis shows the frequency Z and the horizontal axis shows the transmittivity from the system composed of 32 stacking planes of rods. The solid curve shows the transmittivity as a function of Z, in (a) for the range of $0 < Z < 1.0$ and in (b) for $1.0 < Z < 2.0$. The parameters are $a = 0.3d$ and $\varepsilon_< = 3.2^2$. All the calculated photonic bands, Exy as well as Ez, of $\mathbf{k} = (0, k_y, 0)$ are superimposed by the dotted curves as functions of k_y (upper horizontal axis). They are reproduced from Figs. 1(c) and 1(d).

To examine the relation between $T(32)$ and the band structure in more detail in the frequency region $1.0<Z<2.0$, we give in Fig. 6 an enlarged figure for the features in the range $1.4<Z<1.5$, (a) for the z-polarized and (b) for the x-polarized incident light. In the present case of $k_z=0$, the M and N waves are decoupled. The bands shown by the dotted curves in (a) are those of the NN block of the secular equation, which are polarized in the z direction and those from the MM in (b) (Fig. 5 involves all the bands).

One notable feature is that there are optical inactive photonic bands. Within, e.g., the lowest stop bands of both panels, we can see the presence of one band that leaves no trace in the transmittivity. The origin is discussed group theoretically by Stefanou, Karathanos, and Modinos,[44] Robertson *et al.*,[45] and Sakoda.[41] For the group theory of photonic bands, see Ref. 10. We also note that the transmittivity presents a sharp change, wherever an optical-active band terminates. This is the case not only at the edge of every stop band but also within the range of Z where the transmission coefficient is finite. See in Fig. 6 the good correspondence at the positions of the band terminations marked by the arrows. Besides, the interference fringes reflect the curvature of the dispersion curve of an excited band in that the flatter it is, the shorter becomes the periodicity of the oscillation in Z. The transmission of a light, therefore, monitors faithfully the band structure. Finally, Fig. 6 shows that the data needed to have the accuracy of three decimal places to have such a good correspondence. Also, we have calculated the band energies of about 80 bands, to be compared to 10 or 15 bands calculated in the plane-wave method in the literature.

In summary, cylindrical waves are indeed very powerful in the numerical calculation. The results presented above are qualitatively quite similar to those of arrayed dielectric spheres.[8–11]

VI. SUMMARY

In the present paper we give the formulation of the band-structure and transmittivity calculations for the periodic array of dielectric cylinders using the cylindrical waves as basis functions. We have emphasized the role of the completeness relation of the cylindrical waves, which enabled us to arrive at the electromagnetic version of the band calculation almost straightforwardly. The fast convergence is assured by the use of the **t** matrix for the cylindrical partial waves and by the Ewald method in calculating the structure factor. We give the detailed expression for them both. Light transmission and reflection are treated by the layer-doubling method based upon the scattering data of the monolayer of dielectric rods.

The formulation enables us to obtain very accurate data. We showed this in two ways: the check of the convergence of the plane-wave band calculations and the demonstration of a very good correspondence between the transmittivity curve and band structure, both obtained by the cylindrical-wave calculation.

Although we have not examined the eigenvectors obtained by the cylindrical-wave formulation, the experience of the arrayed spherical dielectrics show that they will certainly be of very high quality. This is one of the essential properties required for the eigenvectors to yield an accurate field intensity near and inside the cylinders. Since the step change of

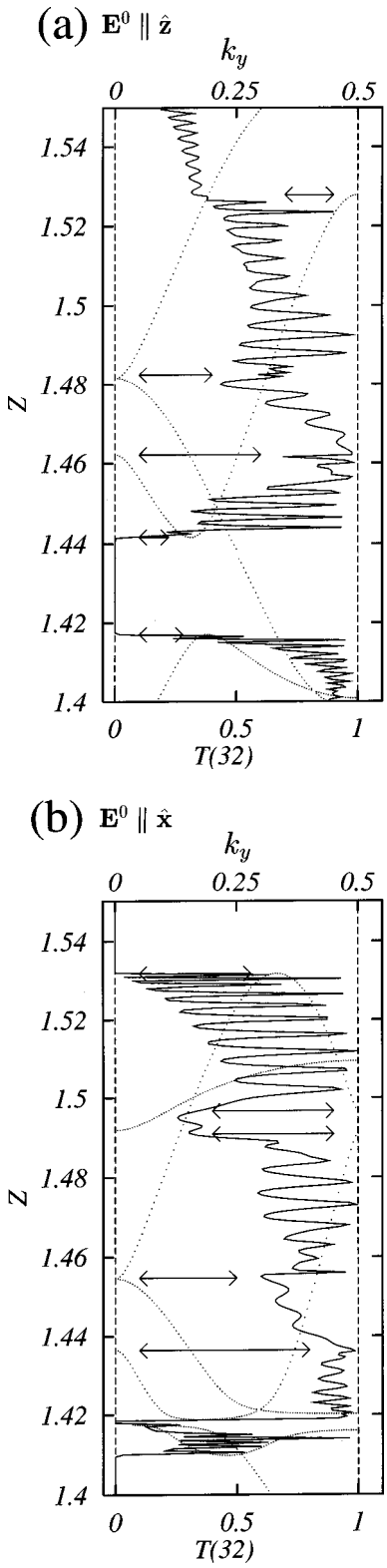

FIG. 6. Transmittivity in the narrow range of $1.4<Z<1.55$, for the z-polarized light in (a) and x-polarized light in (b). The transmittivity of the horizontal axis is shown by the solid curve as a function of Z of the vertical axis. The bands superimposed in (a) by the dotted curves are the Ez bands obtained from the NN block of Eq. (3.56) and those in (b) are the Exy bands obtained from the MM block. At each position of the arrow, the transmittivity curve has a clear trace of the band termination.

the dielectric property at the surface of the rods gives rise to an unwieldy Gibbs phenomena in the plane-wave calculation, the cylindrical-wave formulation will be helpful in many ways other than the convergence of the band calculation.

ACKNOWLEDGMENTS

The authors wish to acknowledge Professor K. Koda for his continuous encouragement and stimulating discussions. This work was supported by the Grant-in Aid for Scientific Research on Priority Area ''Quantum Manipulation of Radiation Field and Matter'' from the Ministry of Education, Science, Sports and Culture of Japan.

APPENDIX A: STRUCTURE FACTOR FOR THE MONOLAYER OF RODS

The essence of the Ewald method, which assures the fast convergence of the lattice sum, is to divide the sum into two parts, and the difficult sum over the remote lattice points is carried out in the reciprocal lattice space. The concept is explained in detail in the book by Born and Huang.[46] The formula listed below for the array of cylindrical rods are simply the modifications of those derived by Kambe for the spherical case.[32]

We start from the plane-wave expansion of the Green's function of the monolayer case given by Eq. (3.32):

$$g^{(0)}(\boldsymbol{\rho},\boldsymbol{\rho}')+g^{(1)}(\boldsymbol{\rho},\boldsymbol{\rho}')=\sum_h \frac{-i}{2d\gamma_h}e^{i(k_x+h)(x-x')+i\gamma_h|y-y'|}$$
$$=\sum_h \frac{1}{2id}\left(\frac{\pi}{2}\frac{|y-y'|}{\gamma_h}\right)^{1/2}H^{(1)}_{-1/2}$$
$$\times(\gamma_h|y-y'|)e^{i(k_x+h)(x-x')}, \tag{A1}$$

with $\boldsymbol{\rho}-\boldsymbol{\rho}'=(x-x',y-y')$. In the second line the definition of the Hankel function of the first kind is used. We take $\mathrm{Im}\gamma_h>0$, when $(\gamma_h)^2<0$.

Using the integral transform for the Hankel function, we can rewrite Eq. (A1) as

$$g^{(0)}(\boldsymbol{\rho},\boldsymbol{\rho}')+g^{(1)}(\boldsymbol{\rho},\boldsymbol{\rho}')$$
$$=\frac{1}{2id}\left(\frac{\pi}{2}\right)^{1/2}\left[\sum_{\substack{h\\ \gamma_h{}^2>0}} e^{i(k_x+h)X}\frac{1}{\pi i}\left(\int_o^w+\int_w^{-\infty}\right)\right.$$
$$\times e^{1/2\left(\gamma_h{}^2t-\frac{|Y|^2}{t}\right)}t^{-1/2}dt+\sum_{\substack{h\\ \gamma_h{}^2<0}} e^{i(k_x+h)X}\frac{1}{\pi i}$$
$$\left.\times\left(\int_o^w+\int_w^{\infty}\right)e^{1/2\left(\gamma_h{}^2t-\frac{|Y|^2}{t}\right)}t^{-1/2}dt\right], \tag{A2}$$

where

$$X=x-x', \quad Y=y-y'. \tag{A3}$$

The parameter w is an important one. It divides the integral over $0<t<\infty$ into two at $t=w$. It may be chosen to be arbitrary and provides a good numerical check in the sense that each of $S^{(k)}(k=1,2,3)$, defined below, depends critically on w but the sum does not. When the two integrals over $0<t<w$ are combined, the integrand of the sum is seen periodic as a function of k_x with periodicity $2\pi/d$. This part is thus resolved into a Fourier series. We find

$$g^{(0)}+g^{(1)}=-\frac{1}{4\pi}\int_{1/w}^{\infty}\frac{1}{u}\sum_n \exp\left[-\frac{1}{2}\left(|\mathbf{R}+x_n\hat{\mathbf{x}}|^2u-\frac{\lambda_>^2}{u}\right)\right.$$
$$\left.-ik_xx_n\right]du-\frac{1}{2\pi d}\left(\frac{\pi}{2}\right)^{1/2}\left[\sum_{\substack{h\\ \gamma_h{}^2>0}} e^{i(k_x+h)X}\int_w^{-\infty}\right.$$
$$\left.+\sum_{\substack{h\\ \gamma_h{}^2<0}} e^{i(k_x+h)X}\int_w^{\infty}\right]e^{1/2\left(\gamma_h{}^2t-\frac{|Y|^2}{t}\right)}t^{-1/2}dt \tag{A4}$$

with

$$\mathbf{R}=(x,y) \tag{A5}$$

and $x_n\hat{\mathbf{x}}$ the center of the nth rod on the x axis given by

$$x_n=nd. \tag{A6}$$

On the other hand, the original definition of Eq. (3.6) leads to

$$g^{(0)}+g^{(1)}=\int\frac{dp_xdp_y}{(2\pi)^2}\frac{\exp[i\mathbf{p}\cdot(\boldsymbol{\rho}-\boldsymbol{\rho}')]}{\lambda_>^2-p_x^2-p_y^2}$$
$$+\sum_n{}' e^{ik_xx_n}\int\frac{dp_xdp_y}{(2\pi)^2}\frac{\exp[i\mathbf{p}\cdot(\boldsymbol{\rho}-\boldsymbol{\rho}'-\mathbf{x}_n)]}{\lambda_>^2-p_x^2-p_y^2}$$
$$=-\frac{i}{4}H_0^{(1)}(\lambda_>|\boldsymbol{\rho}-\boldsymbol{\rho}'|)$$
$$+\sum_n{}' e^{ik_xx_n}\int\frac{dp_xdp_y}{(2\pi)^2}\frac{\exp[i\mathbf{p}\cdot(\boldsymbol{\rho}-\boldsymbol{\rho}'-\mathbf{x}_n)]}{\lambda_>^2-p_x^2-p_y^2}$$
$$=-\frac{i}{4}H_0^{(1)}(\lambda_>|\boldsymbol{\rho}-\boldsymbol{\rho}'|)-\frac{i}{4}\sum_{l=-\infty}^{\infty}J_l(\lambda_>|\boldsymbol{\rho}-\boldsymbol{\rho}'|)$$
$$\times e^{il\theta(\boldsymbol{\rho}-\boldsymbol{\rho}')}S_l. \tag{A7}$$

The constant S_l of the second term is thus related to Green's function via

$$S_l=\frac{4i}{J_l(\lambda_>|\boldsymbol{\rho}-\boldsymbol{\rho}'|)}\int\frac{d\theta(\boldsymbol{\rho}-\boldsymbol{\rho}')}{2\pi}\left[g^{(0)}+g^{(1)}+\frac{i}{4}H_0^{(1)}\right.$$
$$\left.\times(\lambda_>|\boldsymbol{\rho}-\boldsymbol{\rho}'|)\right]e^{-il\theta(\boldsymbol{\rho}-\boldsymbol{\rho}')}. \tag{A8}$$

Since S_l is independent of $\boldsymbol{\rho}-\boldsymbol{\rho}'$, we may derive it by taking the limit $\boldsymbol{\rho}-\boldsymbol{\rho}'\to 0$. The structure factor $\Gamma_{ll'}(k_x,k_z)$ is related to S_l. Comparing Eq. (3.7) with the second term of Eq. (A7), we find

$$\sum_l J_l(\lambda_>|\boldsymbol{\rho}-\boldsymbol{\rho}'|)e^{il\theta(\boldsymbol{\rho}-\boldsymbol{\rho}')}S_l$$

$$=\sum_l \sum_{l'} J_l(\lambda_>\rho)e^{il\theta(\rho)}\Gamma_{ll'}J_{l'}(\lambda_>\rho')e^{-il\theta(\rho')}. \tag{A9}$$

Here we use the following identity on the left-hand side:

$$J_l(\lambda_>|\boldsymbol{\rho}-\boldsymbol{\rho}'|)$$

$$=\sum_{l'l''} J_{l'}(\lambda_>\rho)J_{l''}(\lambda_>\rho')e^{il'\theta(\boldsymbol{\rho})}e^{-il''\theta(\boldsymbol{\rho}')}\delta_{l,l'-l''}. \tag{A10}$$

We then arrive at

$$\Gamma_{l_1l_2}(k_x,k_z)=S_{l_1-l_2}. \tag{A11}$$

Calculation of S_l is due to Eq. (A8) with Eq. (A4) substituted for the Green's function. The term of the sum over the reciprocal lattice point h yields $S_l^{(1)}$, that of the real-space sum with $n\neq 0$ gives $S_l^{(2)}$ and the term $n=0$ leads to $S_l^{(3)}$:

$$S_l=S_l^{(1)}+S_l^{(2)}+S_l^{(3)}, \tag{A12}$$

or

$$\Gamma_{ll'}=S_{l-l'}^{(1)}+S_{l-l'}^{(2)}+S_{l-l'}^{(3)}. \tag{A13}$$

It then holds that

$$S_l^{(1)}=-\frac{i}{d}\left(\frac{2}{\pi}\right)^{1/2} i^l\, l!\sum_h \sum_{l'=0}^{[l/2]} \left(\frac{k_x+h}{\lambda_>}\right)^l$$

$$\times(-1)^{l'}\frac{1}{(l-2l')!\; l'!}\left(\frac{k_x+h}{2}\right)^{-2l'}\left(\frac{1}{8}\right)^{l'}$$

$$\times\left(\frac{\gamma_h{}^2 e^{-\pi i}}{2}\right)^{l'-(1/2)}\Gamma\left(\frac{1}{2}-l',e^{-\pi i}\frac{\Gamma_h{}^2\;\omega}{2}\right), \tag{A14}$$

where $[l/2]$ is the Gauss symbol and the last function is the incomplete γ function, discussed later. $S_l^{(2)}$ is defined by

$$S_l^{(2)}=-(-1)^l\frac{i}{\pi}{\sum_n}'\; e^{-ik_xx_n}\left(\frac{\lambda_>x_n}{2}\right)^l\int_0^{w\lambda_>^2/2}$$

$$\times e^{u-(\lambda_>^2x_n^2/4u)}u^{-l-1}du$$

$$=(-1)^{l+1}\frac{i}{\pi}{\sum_n}'\; e^{ik_xx_n}\left(\frac{\lambda_>x_n}{2}\right)^l I_l \tag{A15}$$

with I_l considered below. The remaining $S_l^{(3)}$ is

$$S_l^{(3)}=\delta_{l0}\left[-1-\frac{i}{\pi}\left\{\gamma+\ln\frac{w\lambda_>^2}{2}+\sum_{k=1}^{\infty}\frac{1}{k!}\left(\frac{w\lambda_>^2}{2}\right)^k\frac{1}{k}\right\}\right] \tag{A16}$$

with the Euler constant $\gamma=0.5772\ldots$.

The incomplete γ function

$$\Gamma(a,x)=\int_x^{\infty}e^{-t}t^{a-1}dt \tag{A17}$$

is obtained from the recursion relation

$$\Gamma(a,x)=\frac{1}{a}[\Gamma(a+1,x)-x^ae^{-x}] \tag{A18}$$

with the start

$$\Gamma\left(\frac{1}{2},x\right)=\begin{cases}\sqrt{\pi}-2\displaystyle\int_0^{\sqrt{x}}e^{-u^2}du & \text{for } x\geqslant 0,\\ \sqrt{\pi}+2i\displaystyle\int_0^{\sqrt{-x}}e^{-u^2}du & \text{for } x<0,\end{cases} \tag{A19}$$

for which we have employed in the numerical application the formula (7.1.26) of Abramovitz and Stegun.[47]

The function I_l of Eq. (A15) is defined by

$$I_l=\int_0^{w\lambda_>^2/2}e^{u-(\lambda_>^2x_n^2/4u)}u^{-l-1}du. \tag{A20}$$

It satisfies

$$\left(\frac{\lambda_>x_n}{2}\right)^2 I_{l+1}=lI_l-I_{l-1}+\left(\frac{\omega\lambda_>^2}{2}\right)^{-l}$$

$$\times\exp\left[\frac{\omega\lambda_>^2}{2}-\frac{\lambda_>^2x_n^2}{4\left(\frac{\omega\lambda_>^2}{2}\right)}\right]. \tag{A21}$$

Introducing

$$p=\lambda^2x_n^2/4,$$

$$q=w\lambda^2/2, \tag{A22}$$

we find

$$I_0=\sum_{k=0}^{\infty}(p^k/k!)\Gamma\left(-k,\frac{p}{q}\right),$$

$$I_1=\sum_{k=0}^{\infty}(p^{k-1}/k!)\Gamma\left(-k+1,\frac{p}{q}\right). \tag{A23}$$

The incomplete γ functions therein are obtained through the recursion formula [Eq. (A18)] with

$$\Gamma(0,z)=E_1(z),$$

$$\Gamma(1,z)=e^{-z}. \tag{A24}$$

For $E_1(z)$ we have used the formulas (5.1.53) and (5.1.56) of the book cited above.

If the parameter w is chosen to be large, the real-space sum over n of $S_l^{(2)}$ [Eq. (A15)] converges slowly. Conversely, if w is small, the sum over h of $S^{(1)}$ [Eq. (A14)] is slowly convergent. The value $w/d^2\sim 1$ was chosen in our calculation, after checking that the sum of $S^{(1)}$, $S^{(2)}$, and $S^{(3)}$ remains constant irrespective of the choice of w in the range $0.2<w/d^2<10$.

Finally the symmetry relation exists between positive and negative l. We find

$$S_{-l}=(-1)^l S_l. \tag{A25}$$

This relation, when used in Eq. (A13), reduces greatly the numerical task.

APPENDIX B: STRUCTURE FACTOR FOR THE BAND CALCULATION

The structure factor of the infinite array of rods is obtained similarly. Let 2D vector $\mathbf{R_n}$ be the center of the rod $\mathbf{n}$ in the xy plane, and $\mathbf{h}$ be a 2D reciprocal lattice vector for the lattice of $\mathbf{R_n}$. The scalar structure factor is still given by Eq. (A13). Of $S^{(1)}$, $S^{(2)}$, and $S^{(3)}$, $S^{(3)}$ is given by Eq. (A16). The others are simplified greatly. To summarize,

$$S_l^{(1)}=4i^{l+1}\sum_{\mathbf{h}}\frac{1}{v_c}\left[\frac{|\mathbf{k}_\perp+\mathbf{h}|}{\lambda_>}\right]^l e^{w\lambda_>^2/2}e^{-il\theta(\mathbf{k}_\perp+\mathbf{h})} \times\frac{\exp\left[-(\mathbf{k}_\perp+\mathbf{h})^2\frac{w}{2}\right]}{\lambda_>^2-(\mathbf{k}_\perp+\mathbf{h})^2},$$

$$S_l^{(2)}=-\frac{i}{\pi}{\sum_{\mathbf{n}}}'\left(\frac{\lambda_>|\mathbf{R_n}|}{2}\right)^l\exp(i\mathbf{k}_\perp\cdot\mathbf{R_n})\ e^{-il\theta(\mathbf{R_n})} \times I_l(x_n^2\to|\mathbf{R_n}|^2),$$

$$S_l^{(3)}=\delta_{l0}\left[-1-\frac{i}{\pi}\left\{\gamma+\ln\frac{w\lambda_>^2}{2}+\sum_{k=1}^{\infty}\frac{1}{k!}\left(\frac{w\lambda_>^2}{2}\right)^k\frac{1}{k}\right\}\right]. \tag{B1}$$

In $S_l^{(2)}$, the argument of x_n^2 of I_l [Eq. (A20)] must be changed to $|\mathbf{R_n}|^2$. The two angles in Eq. (B1) are defined by

$$\theta(\mathbf{k}_\perp+\mathbf{h})=\tan^{-1}[(k_y+h_y)/(k_x+h_x)],$$

$$\theta(\mathbf{R_n})=\tan^{-1}[y_n/x_n]. \tag{B2}$$

The choice of $w/d^2\simeq 1.0$ was found practical.

The symmetry of $S^{(k)}$ is found to be

$$S_{-l}^{(k)}=-[S_l^{(k)}]^* \tag{B3}$$

for $k=1,2$.

Finally, there occurs a situation in the band calculation, where $\lambda_>^2<0$. This can happen because, for a band energy of $\mathbf{k}$ with a positive $\lambda_<^2$, Eqs. (3.16) and (3.17) yield

$$\lambda_>^2=(\lambda_<^2+k_z^2)/\varepsilon_<-k_z^2 \tag{B4}$$

and the right-hand side can be negative for a large $\varepsilon_<$. In this case, $\lambda_>$ in Eq. (B1) must be changed everywhere by $e^{i\pi/2}|\lambda_>|$ [in Eqs. (3.23), too, this replacement is necessary]. The logarithm of $S^{(3)}$, for example, then becomes complex with an imaginary part of $+i\pi$. The symmetry in this situation is ($k=1,2$),

$$S_{-l}^{(k)}=-(-1)^l[S_l^{(k)}]^*. \tag{B5}$$

APPENDIX C: STRUCTURE FACTOR FOR A COMPLEX LATTICE OF RODS

The formulas for a complex lattice of parallel rods whose unit cell contain several dielectric rods are given here. In the secular equation given by Eq. (3.56), the rows and columns of the matrices are now labeled β, l, and s, with s specifying the number of the rods in the unit cell. Let $\mathbf{r}_s$ be the 2D position of the center of the sth rod in the xy plane. Then

$$[\mathbf{D}^{<(>)}(ss')]_{ll'}=d_l^{<(>)}(s)\,\delta_{ll'}\delta_{ss'},$$

$$[\mathbf{\Gamma}(ss')]_{ll'}=\Gamma_{ll'}(ss'). \tag{C1}$$

For each pair (ss'), Eq. (3.45) still holds. The quantity $d_l^{<(>)}(s)$ is obtained from Eq. (3.23) by using a and $\varepsilon_<$ of the sth rod. For the scalar structure factor, Eq. (A13) is changed to

$$\Gamma_{ll'}(ss')=S_{l-l'}^{(1)}(ss')+S_{l-l'}^{(2)}(ss')+S_{l-l'}^{(3)}(ss'). \tag{C2}$$

The three $S^{(k)}$'s are obtained as

$$S_l^{(1)}(ss')=4i^{l+1}\sum_{\mathbf{h}}\frac{1}{v_c}\left[\frac{|\mathbf{k}_\perp+\mathbf{h}|}{\lambda_>}\right]^l e^{w\lambda_>^2/2}e^{-il\theta(\mathbf{k}_\perp+\mathbf{h})} \times\frac{\exp\left[-(\mathbf{k}_\perp+\mathbf{h})^2\frac{w}{2}\right]}{\lambda_>^2-(\mathbf{k}_\perp+\mathbf{h})^2}\exp[i(\mathbf{k}_\perp+\mathbf{h})\cdot\mathbf{r}_{ss'}],$$

$$S_l^{(2)}(ss')=-\frac{i}{\pi}{\sum_{\mathbf{n}}}''\left(\frac{\lambda_>|\mathbf{R_n}-\mathbf{r}_{ss'}|}{2}\right)^l\exp(i\mathbf{k}_\perp\cdot\mathbf{R_n}) \times e^{-il\theta(\mathbf{R_n}-\mathbf{r}_{ss'})}I_l(x_n^2\to|\mathbf{R_n}-\mathbf{r}_{ss'}|^2),$$

$$S_l^{(3)}(ss')=\delta_{ss'}\delta_{l,0}\left[-1-\frac{i}{\pi}\left\{\gamma+\ln\frac{w\lambda_>^2}{2} +\sum_{k=1}^{\infty}\frac{1}{k!}\left(\frac{w\lambda_>^2}{2}\right)^k\frac{1}{k}\right\}\right], \tag{C3}$$

with

$$\mathbf{r}_{ss'}=\mathbf{r}_s-\mathbf{r}_s' \tag{C4}$$

and

$${\sum_{n}}''=\begin{cases}\displaystyle\sum_{n\neq 0} & \text{for } s=s',\\ \displaystyle\sum_{n=\text{ all}} & \text{for } s\neq s'.\end{cases} \tag{C5}$$

In $S^{(2)}$ the replacement of the argument in I_l must be made in Eq. (A20). The symmetry between the positive and negative l turns out to be ($k=1,2$)

$$S_{-l}^{(k)}(ss')=-[S_l^{(k)}(s's)]^*, \tag{C6}$$

when $\lambda_>^2>0$ and

$$S_{-l}^{(k)}(ss')=-(-1)^l[S_l^k(s's)]^*, \tag{C7}$$

when $\lambda_>^2<0$.

*Electronic address: ohtaka@j90.tg.chiba-u.ac.jp

[1] E. Yablonovitch, Phys. Rev. Lett. **58**, 2059 (1987). For review articles of the general aspects of photonic bands, see, e.g., E. Yablonovitch, in *Photonic Band Gaps and Localization*, edited by C. M. Soukoulis (Plenum, New York, 1993), p. 207; J. Phys.: Condens. Matter **5**, 2443 (1993); see also, J. D. Joannopoulos, R. D. Meade, and J. N. Winn, *Photonic Crystals* (Princeton University Press, Princeton, 1955); and P. M. Hui and Neil F. Johnson, in *Solid State Physics*, edited by H. Ehrenreich and F. Spaepen (Academic, New York, 1995), Vol. 49, p. 151.

[2] Z. Zhang and S. Satpathy, Phys. Rev. Lett. **65**, 2650 (1990). Many more recent works are found in J. Opt. Soc. Am. **10** (1993). See also the works in *Photonic Band Gaps and Localization*, edited by C. M. Soukoulis (Plenum, New York, 1993); and in *Photonic Band Gap Materials* (Kluwer, Dordrecht, 1996), edited by C. M. Soukoulis.

[3] D. L. Mills and S. E. Trullinger, Phys. Rev. B **36**, 947 (1987).

[4] G. Kurizki and A. Z. Genack, Phys. Rev. Lett. **61**, 2269 (1988).

[5] S. John and N. Aközbek, Phys. Rev. Lett. **71**, 1168 (1993).

[6] S. John and T. Quang, Phys. Rev. A **50**, 1764 (1994); Phys. Rev. Lett. **74**, 3419 (1995).

[7] K. Sakoda and K. Ohtaka, Phys. Rev. B **54**, 5732 (1996); **54**, 5742 (1996).

[8] K. Ohtaka and Y. Tanabe, J. Phys. Soc. Jpn. **65**, 2265 (1996).

[9] K. Ohtaka and Y. Tanabe, J. Phys. Soc. Jpn. **65**, 2670 (1996).

[10] K. Ohtaka and Y. Tanabe, J. Phys. Soc. Jpn. **65**, 2276 (1996).

[11] K. Ohtaka, T. Ueta, and Y. Tanabe, J. Phys. Soc. Jpn. **65**, 3068 (1996).

[12] Y. Yamagami and A. Hasegawa, J. Phys. Soc. Jpn. **60**, 987 (1991).

[13] See, e.g., H. M. Tzeng, K. F. Wall, M. B. Long, and R. K. Chang, Opt. Lett. **9**, 499 (1984); J. D. Eversole, H.-B. Lin, A. L. Huston, A. J. Campillo, P. T. Leung, S. Y. Liu, and K. Young, J. Opt. Soc. Am. B **10**, 1955 (1993), and references therein.

[14] S. John and J. Wang, Phys. Rev. Lett. **64**, 2418 (1990).

[15] S. L. McCall, P. M. Platzman, R. Dalichaouch, D. Smith, and S. Schultz, Phys. Rev. Lett. **67**, 2017 (1991).

[16] J. W. Haus, J. Mod. Opt. **41**, 195 (1994), and references therein.

[17] S. Bulgakov and M. Nieto-Vesperinas, J. Opt. Soc. Am. A **13**, 500 (1996).

[18] N. A. Nicorovici and R. C. McPhedran, Phys. Rev. E **50**, 3143 (1994).

[19] N. A. Nicorovici, R. C. McPhedran, and Bao Ke-Da, Phys. Rev. E **51**, 690 (1995).

[20] N. A. Nicorovici, R. C. McPhedran, and L. C. Botten, Phys. Rev. E **52**, 1135 (1995).

[21] K. Ohtaka, Phys. Rev. B **19**, 5057 (1979).

[22] H. S. Sözüer, J. W. Haus, and R. Inguva, Phys. Rev. B **45**, 13 962 (1992).

[23] J. A. Stratton, *Electromagnetic Theory* (McGraw-Hill, New York, 1941), p. 397.

[24] J. D. Jackson, *Classical Electrodynamics*, 2nd ed. (Wiley, New York, 1975), p. 739.

[25] K. Ohtaka, J. Phys. C **13**, 667 (1980).

[26] R. Ruppin and R. Englman, Rep. Prog. Phys. **33**, 149 (1970).

[27] J. B. Pendry, *Low Energy Electron Diffraction* (Academic, London, 1974), p. 138.

[28] S. Y. Tong, Prog. Surf. Sci. **7**, 1 (1975).

[29] J. B. Pendry, J. Mod. Opt. **41**, 209 (1993).

[30] D. Felbacq, G. Tayeb, and D. Maystre, J. Opt. Soc. Am. A **11**, 2526 (1994).

[31] K. Ohtaka and M. Inoue, J. Phys. Soc. Jpn. **52**, 3853 (1983).

[32] K. Kambe, Z. Naturforsch. A **22**, 322 (1967).

[33] F. S. Ham and B. Segall, Phys. Rev. **124**, 1786 (1961).

[34] J. W. Haus, H. S. Sözüer, and R. Inguva, J. Mod. Opt. **39**, 1991 (1992); H. S. Sözüer and J. W. Haus, J. Opt. Soc. Am. B **10**, 296 (1993).

[35] K. M. Leung and Y. F. Liu, Phys. Rev. Lett. **21**, 2645 (1990).

[36] K. M. Ho, C. T. Chan, and C. M. Soukoulis, Phys. Rev. Lett. **65**, 3152 (1990).

[37] C. M. Anderson and K. P. Giapis, Phys. Rev. Lett. **30**, 2949 (1996), and references therein.

[38] M. Plihal and A. A. Maradudin, Phys. Rev. B **44**, 8565 (1991).

[39] P. R. Villeneuve and M. Piché, *Photonic Band Gaps and Localization*, edited by C. M. Soukoulis (Plenum, New York, 1993), p. 283.

[40] A. A. Maradudin and A. R. McGurn, *Photonic Band Gaps and Localization*, edited by C. M. Soukoulis (Plenum, New York, 1993), p. 247; J. Opt. Soc. Am. B **10**, 307 (1993).

[41] K. Sakoda, Phys. Rev. B **52**, 7982 (1995).

[42] K. Sakoda, Phys. Rev. B **51**, 4672 (1995); **52**, 8992 (1995).

[43] K. Sakoda (private communication).

[44] N. Stefanou, V. Karathanos, and A. Modinos, J. Phys.: Condens. Matter **4**, 7389 (1992).

[45] W. M. Robertson, G. Arjavalingam, R. D. Meade, K. D. Brommer, A. M. Rappe, and J. D. Joannopoulos, Phys. Rev. Lett. **68**, 2023 (1992); J. Opt. Soc. Am. B **10**, 322 (1993).

[46] M. Born and K. Huang, *Dynamical Theory of Crystal Lattices* (Oxford University Press, London, 1968), p. 385.

[47] M. Abramowitz and I. A. Stegun, *Handbook of Mathematical Functions* (Dover, New York, 1970), p. 295.